POTSDAM-INSTITUT FÜR KLIMAFOLGENFORSCHUNG

Comparison and Correction of High-Mountain Precipitation Data Based on Glacio-Hydrological Modeling in the Tarim River Headwaters (High Asia)

MICHEL WORTMANN

Potsdam Institute for Climate Impact Research, Potsdam, Germany

TOBIAS BOLCH

Department of Geography, University of Zurich, Zurich, Switzerland

CHRISTOPH MENZ

Potsdam Institute for Climate Impact Research, Potsdam, Germany

JIANG TONG

National Climate Centre, Chinese Meteorological Administration, Beijing, China

VALENTINA KRYSANOVA

Potsdam Institute for Climate Impact Research, Potsdam, Germany

(Manuscript received 20 June 2017, in final form 29 March 2018)

ABSTRACT

Mountain precipitation is often strongly underestimated as observations are scarce, biased toward lower-lying locations and prone to wind-induced undercatch, while topographical heterogeneity is large. This presents serious challenges to hydrological modeling for water resource management and climate change impact assessments in mountainous regions of the world, where a large population depends on water supply from the mountains. The headwaters of the Tarim River, covering four remote and highly glacierized Asian mountain ranges, are vital water suppliers to large agricultural communities along the Taklamakan Desert, northwest China. Assessments of future changes to these water towers have been hampered because of the large precipitation uncertainties. In this study, six existing precipitation datasets (observation-based reanalysis datasets, satellite observation datasets, and the output of high-resolution regional climate models) were compared over five headwaters of the Tarim River. The dataset incorporating the highest observation density (APHRODITE) is then corrected by calibrating the glacio-hydrological model Soil and Water Integrated Model–Glacier Dynamics (SWIM-G) to observed discharge, glacier hypsometry, and modeled glacier mass balance. Results show that this form of inverse modeling is able to inform the precipitation correction in such data-scarce conditions. Substantial disagreement of annual mean precipitation between the analyzed datasets, with coefficients of variation in catchment mean precipitation of 68% on average, was found. The model-based precipitation estimates are on average 1.5–4.3 times higher than the APHRODITE data, but fall between satellite-based and regional climate model results.

1. Introduction

Many arid and desert regions in Asia are highly dependent on water resources generated in the mountainous headwaters of High Mountain Asia (High Asia), such as the Indus, Syr Darya, Amu Darja, and the Tarim River (Kaser et al. 2010; Pritchard 2017; Bolch 2017). The latter has China's largest endoheric river basin encircling the Taklamakan Desert. Approximately 10 million people depend on a vast irrigation agriculture along the rivers that provides subsistence farming and produces large shares of China's cotton and fruits (Thevs 2011; Tao et al. 2011; Feike et al. 2015; Rumbaur et al. 2015). The mountain streams originate as either summer rain, snow, or glacier melt in the Karakoram,

Supplemental information related to this paper is available at the Journals Online website: https://doi.org/10.1175/JHM-D-17-0106.s1.

Corresponding author: Michel Wortmann, wortmann@pik-potsdam.de

DOI: 10.1175/JHM-D-17-0106.1

Pamir, Kunlun Shan, and Tien Shan ranges. Despite their importance to downstream communities, the water cycle of the Tarim River and in High Asia in general is poorly gauged and understood (Hewitt 2005; Immerzeel et al. 2012a; Ragettli et al. 2013; Winiger et al. 2005).

The region's high-mountain precipitation is determined by a combination of synoptic climate patterns and small-scale orographic precipitation, resulting in highly heterogeneous and localized precipitation fields (Barry 2008). Most of the moisture arriving in the highly continental Tarim basin is driven by the westerlies and the southwestern Indian monsoon creeping over the Karakoram range in the most southwestern part (Aizen et al. 1995; Mölg et al. 2014; Yao et al. 2012). The combination of a sparse meteorological station density and topographical heterogeneity spell an unrelenting data scarcity for any kind of water resource assessment. The few meteorological stations that exist are mostly located at more accessible, low-lying locations in valley bottoms and at the populated edge of the Taklamakan Desert (Tao et al. 2011). This introduces a measurement bias with a tendency to much drier conditions, a situation common in mountain regions around the world (De Jong et al. 2005).

A further precipitation bias is introduced by gauge undercatch, which is especially important in mountainous regions because of strong winds and high proportions of solid precipitation (Yang et al. 1999; Adam et al. 2006; Groisman et al. 1991). For example, unshielded precipitation gauges may collect less than 50% of actual solid precipitation at high wind speeds (Kochendorfer et al. 2017; Yang and Ohata 2001). Overcoming these sources of negative bias for accurate water resource assessments is a challenge, but promising recent advances such as high-resolution satellite-based precipitation measurements and better glacier inventories need to be utilized.

There have been numerous studies on observed changes in the Tarim basin's climate, but they largely fail to address mountain precipitation. A general increasing trend of both precipitation and temperature has been observed in the last decades (Changchun et al. 2008; Chen et al. 2006; Tao et al. 2011; Fan et al. 2011) with especially the Tarim River's most important tributary, the Aksu River, experiencing an increase in discharge (Wang et al. 2008; Krysanova et al. 2015). AVHRR and MODIS remotely sensed snow cover area at high elevations has been investigated and was shown to have undergone only mild changes over the past three decades (Peters et al. 2015). Changchun et al. (2008) detected slight increases in snow cover area and significant correlation with precipitation variability, but none with temperature. None of these observation-based studies have addressed precipitation biases in the Tarim River's headwaters, where the vast majority of the region's freshwater is generated and estimates of annual total catchment precipitation are absent.

The recent availability of spatially distributed precipitation products, observation-based interpolations, and reanalysis datasets has provided hydrological modelers with convenient input data, but they largely inherit the low-elevation bias of their boundary conditions, and differences between station densities exist (Lorenz and Kunstmann 2012). Prominent examples of global coverage at 0.5° resolution are the ERA-40/ERA-Interim (Dee et al. 2011) and Global Precipitation Climatology Centre (GPCC; Schneider et al. 2015) datasets, which have themselves been used for reanalysis (Weedon et al. 2011). A regional dataset for Asia with the highest station density is APHRODITE at 0.25°–0.5° resolution (Yatagai et al. 2012). Tong et al. (2014) compared some of these precipitation datasets over the Tibetan Plateau and several southeast draining headwaters to station observations and found considerable variability. A major problem in mountainous regions with these datasets is their relatively coarse grids (0.25°–2°), which are a poor match for the complex and poorly represented process of orographic precipitation in those reanalysis models (You et al. 2012; Böhner 2006).

An improvement comes from recent satellite-based products of the Tropical Rainfall Measurement Mission (TRMM) that provide indirect measurements for each grid cell and are extended through modeling. Although it relies on algorithms that are mostly ill suited for small-scale, solid, or short precipitation events (Bookhagen and Burbank 2006; Huffman 2006), it at least performs a spatially homogeneous sampling, and improvements are being made in resolution, algorithms, and sensors (Smith et al. 2007). Another type of precipitation product comes from dynamical, regional climate models that downscale global products to finer resolutions. They are relatively rare, but one exists for the Tibetan Plateau and surrounding mountain ranges with simulations since 2000. The High Asia Refined analysis (HAR) dataset provides detailed and process-based precipitation fields at a 10-km resolution (and 30 km for greater High Asia), but only for 2000–14 (Maussion et al. 2014). It provides valuable estimates of high-altitude water fluxes that are independent from observations. Although a variety of both simulated and observation-based datasets is available, no assessments exist for the data-scarce Tarim River headwaters to determine catchment-wide precipitation relevant for modeling efforts.

While hydrological models use precipitation as a driving variable, they have also been instrumental in verifying catchment-wide precipitation estimates by

calibrating them to available discharge observations. Orographic precipitation is traditionally estimated using linear elevation gradients, similar to temperature. However, they can be highly local and variable with elevation zone and thus rely on an acceptable station network (Sevruk and Mieglitz 2002). Inverse modeling has been used to utilize discharge observations and correct precipitation accordingly (Valéry et al. 2009; Duethmann et al. 2013; Henn et al. 2016). Although it relies heavily on the accurate modeling of other water balance components (most notably evapotranspiration), discharge records often provide the best available evidence in data-scarce regions for catchment precipitation that is higher than meteorological observations suggest. Using information on snow cover has been shown to improve the estimates significantly (Henn et al. 2016; Duethmann et al. 2014). For example, Henn et al. (2015) estimate basinwide precipitation totals using a Bayesian approach and several hydrological models. It was shown in a follow-up study that uncertainties are reduced by one-third if snow water equivalent information is included (Henn et al. 2016).

An important drawback of this method in glacierized regions is the added or withheld discharge from potentially negative or positive glacier mass balances, so those must be known or reasonably constrained. If that is possible, glaciers may even function as gauges of high-altitude precipitation by inverse glacier modeling, which is shown by studies in the Indus basin (Immerzeel et al. 2012b, 2015). By estimating glacier melt, the water balance of individual glacier catchments is closed and local precipitation gradients between glacier accumulation zone and nearby meteorological stations as inferred. To accurately estimate catchment precipitation in the poorly gauged Tarim headwaters, these are promising approaches that have not been tested in existing models.

A similar modeling approach is proposed here to untangle the complexities of underestimated precipitation and glacier mass balances and to provide precipitation estimates that are based on a reasonable glacier and water balance.

2. Study area, data, and methods

a. The Tarim River headwaters

The Tarim River has one of the largest endorheic catchments of the world with a size of about 800×10^3 km^2. As the catchment encompasses the Taklamakan Desert and various salt lakes, the hydrologically active catchment is less than half the area. The river is fed by three large tributaries with their confluence at the northern edge of the desert: the Aksu River originating in the central Tien Shan to the north, the Hotan River originating in the Kunlun Shan to the south, and the Yarkant River originating in the Karakoram and the eastern Pamir (see Fig. 1). As the desert climate in the lower parts of these tributaries produces virtually no river runoff (except for rare extreme rain events; annual potential evapotranspiration exceeds precipitation by a factor of 30–50), the vast majority of river discharge is generated in the glacierized, mountainous headwaters. This study focuses on the five catchments of the gauging stations that are situated at the boundary of the Taklamakan Desert, that is, before river abstractions and significant transmission losses occur (Fig. 1, Table 1).

The climate of the headwaters is highly continental with a strong seasonality governed by the westerlies (Aizen et al. 1995; Maussion et al. 2014). River regimes exhibit a strong peak in summer when snow and ice melt coincides with the precipitation peak. In the Aksu catchment, about 80% of precipitation is measured between the months of April and September. Yarkant and Hotan catchments receive about 60%–70% of precipitation over the same period, as the westerlies remain active in winter in the southwestern parts of the domain (Karakoram). Mean summer (winter) temperatures fall between 3° and 16°C (between −22° and −9°C; Weedon et al. 2011). Precipitation gauge stations in the catchments are sparse (further discussed below). The reanalysis dataset APHRODITE (Yatagai et al. 2012) that incorporates most of them indicates annual totals of 230–314 mm a^{-1} in the Aksu catchments and 62–113 mm a^{-1} in the Hotan and Yarkant catchments.

The mountain ranges surrounding the Taklamakan Desert comprise steep, high-altitude terrain that has given rise to an extensive glacier cover accounting for significant proportions of the catchment areas considered here (Table 1). The mean elevation of the Aksu catchments is 3500 m MSL and includes the highest peak of the Tian Shan, the Jengish Chokuso (Pik Pobedy in Russian or Tömür in Uyghur) at 7439 m MSL. The two catchments cover a total glacier area of about 3350 km^2 (≈2008; Pieczonka and Bolch 2015; Osmonov et al. 2013). A unique glaciological feature of the Aksu headwaters is the ice-dammed Merzbacher Lake that sends near-annually reoccurring subglacial outburst floods (jökulhlaups) downstream with consequences for communities and modeling efforts (Glazirin 2010; Wortmann et al. 2014). The two catchments of the Hotan River span the northwestern edge of the Tibetan Plateau at a mean elevation of 4695 m MSL, including the Liushi Shan at 7167 m MSL, the highest summit of the Kunlun Shan range. Glaciers cover some 5880 km^2 (≈2010) and are mostly cold-based at very high altitudes (Shangguan et al. 2007). The

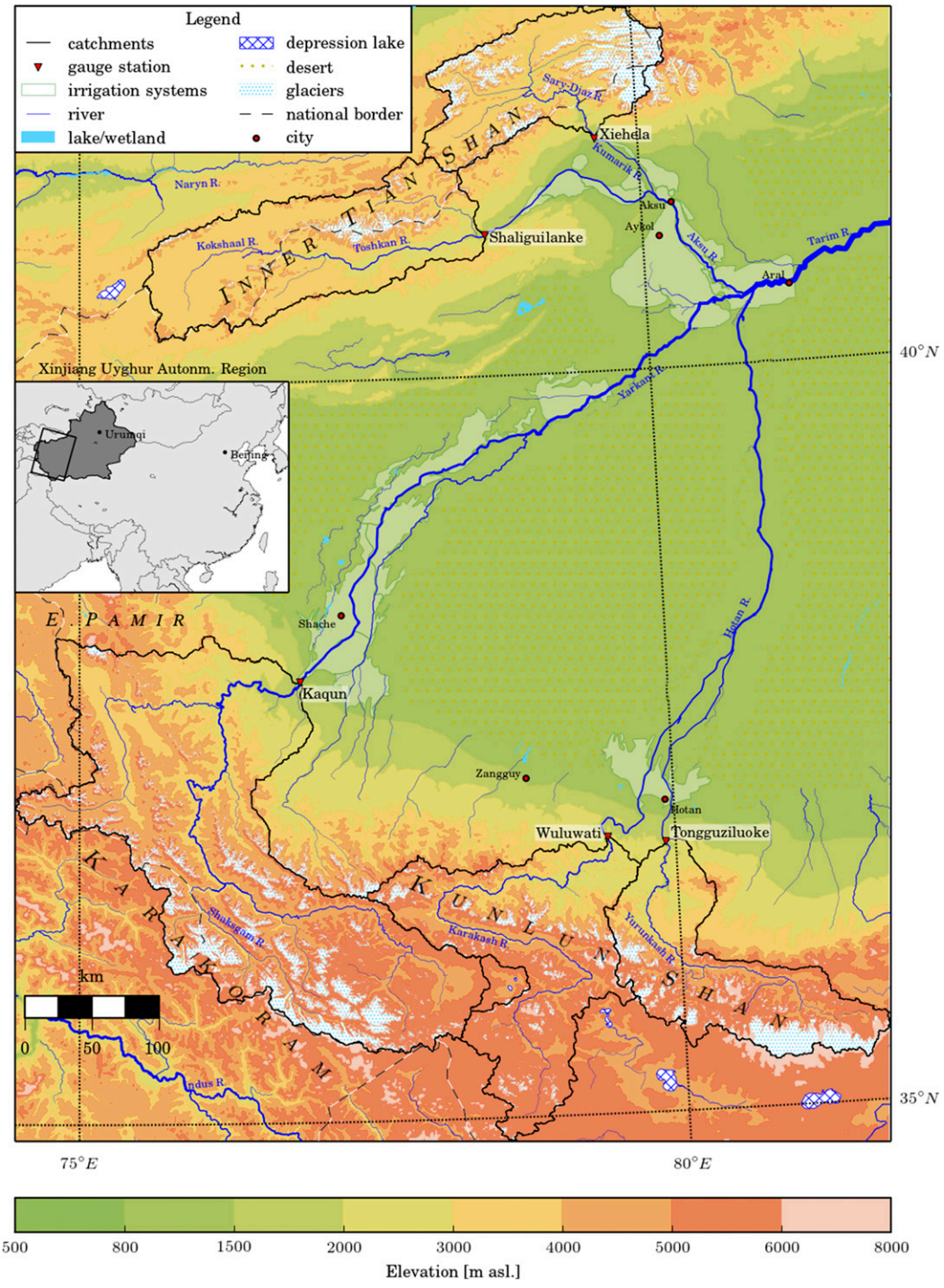

FIG. 1. Map of the five considered catchments that supply the vast majority of discharge to the Tarim River including the large agricultural areas downstream. Figure 2 provides approximate observation station densities. Catchments are referred to in the text by either their outlet station or collectively by their principle river (Aksu, Hotan, Yarkant). See Table 1 for catchment details.

Yarkant headwater catchment has an average elevation of 4425 m MSL with the Karakoram in the south, including the K2 at 8614 m MSL, and the East Pamir in the north. A total glacier area of about 5610 km^2 (2010) is found within the catchment at extremely high and steep altitudes (Frey et al. 2014).

TABLE 1. Catchment statistics for all considered stations with annual and June–August mean discharge Q (data from Chinese Hydrological Yearbooks; Wang 2006) over the period with available data and glacier cover of ≈2008 by Pieczonka and Bolch (2015) and Duethmann et al. (2015).

River	Station	Drainage area (km^2)	Mean Q ($m^3 s^{-1}$)	Mean JJA Q ($m^3 s^{-1}$)	Glacier cover (%)
Aksu	Xiehela	12 989	146.7	406.6	19.8
	Shaliguilanke	18 408	84.4	208.1	4.3
Hotan	Wuluwati	20 600	71.4	200.5	7.5
	Tongguziluoke	14 890	71.1	223.3	22.8
Yarkant	Kaqun	46 759	208.9	578.7	10.3

The Tarim headwaters suffer from severe data scarcity due to the high-altitude, heterogeneous terrain, the associated inaccessibility, and very sparse population. Long-term meteorological stations are therefore extremely difficult to maintain and are scarce. Moreover, the mountain climate exhibits strong vertical gradients (e.g., temperature stratification and orographic precipitation), leading to microclimates and short correlation distances (Beniston 2006). The few meteorological stations are disproportionately located in valley or low-altitude locations (or worse still, at the edge of the Taklamakan Desert; Tao et al. 2011). This introduces a low-altitude bias in the climate data, which leads especially to underestimations of precipitation, making some form of correction and extrapolation necessary (Immerzeel et al. 2012b).

b. *Precipitation datasets*

Six precipitation datasets were selected that cover all five catchments (Table 2). They may be broadly distinguished by the manner in which they assimilate observations and produce distributed precipitation fields. APHRODITE and GPCC use direct precipitation ground observations and are thus referred to as direct precipitation datasets (DPD). The satellite-based datasets TRMM Multisatellite Precipitation Analysis (TMPA) 3B42v7 and Global Precipitation Measurement (GPM) 3IMERGM, as well as the ERA-Interim reanalysis dataset, assimilate mainly indirect observations from space (radiance, sea surface temperature) and some ground-based datasets. We refer to them as satellite-based precipitation datasets (SPD). ERA-Interim falls into this category because it is mainly driven by indirect satellite measurements and does not assimilate direct precipitation observations. A third category includes the COSMO Community Land Model (CCLM) and HAR datasets that are results of regional climate models. They only use global climate model results as boundary conditions. We refer to them as model-based precipitation datasets (MPD).

The six datasets were chosen to assess the region's precipitation by means of all common sources (direct observations, satellites, and climate models). This range allows an adequate evaluation of uncertainties associated with precipitation data available to hydrological modelers for such data-scarce, mountainous catchments, as has been done for other high mountain regions (Tong et al. 2014; Henn et al. 2018). The gridded precipitation dataset of the Chinese Meteorological Administration (CMA) was not considered because it only covers the Chinese territory and is similar in quality to the APHRODITE dataset. We only describe the APHRODITE dataset here because it was used in the calibration of the hydrological model and is generally considered the best dataset available for the region (Tong et al. 2014; Lutz et al. 2014). The others are described in the online supplemental material.

The APHRODITE dataset is a gridded, daily precipitation interpolation of the densest gauge network in

TABLE 2. Selected precipitation datasets with temporal coverage, spatial resolution over the catchments, boundary conditions, and references. The HAR dataset is available in two resolutions, but the finer one only covers the Hotan and Yarkant catchments.

Name	Period	Resolution	Boundary conditions	Reference
APHRODITE	1951–2007	0.25°/0.5°	Point observations	Yatagai et al. (2012)
GPCC	1901–2010	0.5°	Point observations	Schneider et al. (2015)
TMPA/GPM	1998–present	0.25°/0.1°	Radar data from multiple satellites	Liu (2015); Huffman et al. (2014)
ERA-Interim	1979–present	0.5°	Satellite and point observations	Dee et al. (2011)
CCLM	1959–2001	0.44°	ERA-40	Rockel et al. (2008)
HAR	2001–14	10 km/30 km	GFS-FNL	Maussion et al. (2014)

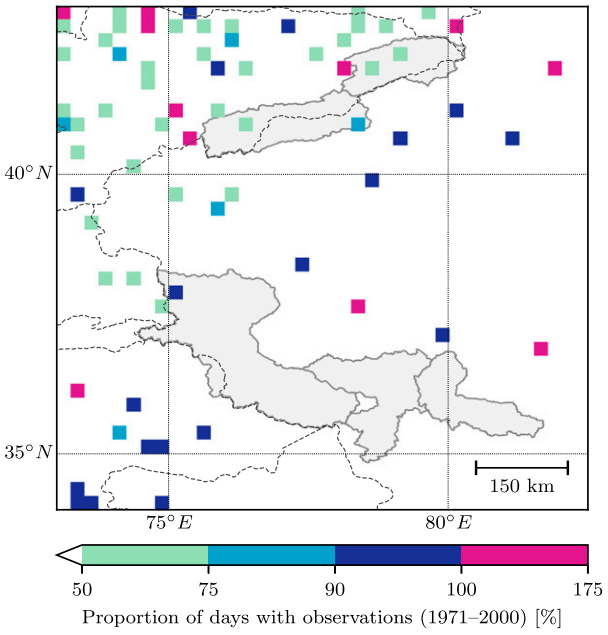

FIG. 2. Precipitation observations in the Tarim headwaters as assimilated into the APHRODITE dataset. Values are percent of days with observations in the period 1970–2000 in each grid cell, i.e., they indicate approximate locations of stations. Cells with more than 100% indicate multiple, simultaneous observations within this cell. Refer to Fig. 1 for elevations.

Asia (Yatagai et al. 2012). A Sheremap-type interpolation scheme was employed to construct daily 0.25° and 0.5° precipitation fields, considering dominant wind exposition and monthly varying correlation distances. While they are the best data available, the underlying station density is still extremely poor, as illustrated in Fig. 2. The Hotan catchments are devoid of any gauging stations, with the closest stations located at the edge of the Taklamakan Desert (see also Tao et al. 2011). Similarly, the Kaqun (Yarkant) catchment has only one station within the catchment boundary, with most surrounding stations at significantly lower-lying locations. The Karakoram range in the southwest of the catchment is particularly remote from any stations.

Despite the drawbacks of APHRODITE, it is the best dataset available for longer-term hydrological modeling, as it covers more than five decades and has a high correlation with observed discharge (in comparison, e.g., to the MPD). The comparison is focused on annual mean precipitation as it summarizes gauging biases well in a highly seasonal climate and is available in all datasets.

c. SWIM-G

The glacio-hydrological model Soil and Water Integrated Model–Glacier Dynamics (SWIM-G) was used to simulate both glacier and the catchment hydrology in a tightly integrated approach (Wortmann et al. 2016). SWIM-G was developed to overcome the conflict of scale between individual glaciers and the catchment hydrology when modeling larger, highly glacierized, typically data-scarce catchments. It relies on computational units that disaggregate complex terrain into parts of similar elevation, aspect, and hydrological subbasin as opposed to gridded (fully distributed) or empirical approaches (e.g., Immerzeel et al. 2012a; Huss et al. 2010). The units are conceptually similar and computationally equal to the hydrological response units (HRUs), enabling a tight integration between the glaciological and hydrological model over large catchments. Typical topographical properties govern the disaggregation considering the catchment characteristics and the desired level of detail. These properties are elevation zones with intervals of 100 m, four aspect classes, and the subbasin boundaries.

The mass balance is evaluated through snow accumulation based on a threshold temperature and an enhanced degree-day melting approach. The latter accounts aspect and terrain shading, debris melt-out, and sublimation. Like most hydrological processes, the glacier processes are computed daily for each unit, and ice is routed laterally between them according to an adapted Glen's Flow Law approach (Marshall et al. 2011). More detail on the model and the specific input data for the Tarim catchments is provided in the supplemental material.

d. Precipitation correction

Where meteorological information has to be extrapolated over great distances both horizontally and/or vertically, a method to correct for orographic precipitation is paramount to the accurate modeling of both the glaciers and the catchment hydrology (Immerzeel et al. 2014; Stisen et al. 2012). Glacio-hydrological models have proven to be useful tools in finding accurate correction factors and gradients with elevation when a near-glacier equilibrium is assumed or mass balances are known (Immerzeel et al. 2012b, 2015).

Most studies use linear gradients to vary precipitation with elevation over a complex terrain with typical ranges of 0.05%–0.5% m^{-1} (Sevruk and Mieglitz 2002; Hock and Holmgren 2005; Immerzeel et al. 2014). However, representing variance of precipitation as a linear function of elevation is inherently local, highly variable over varying altitude ranges, and generally unsuitable for elevations below the reference altitude, as precipitation would diminish to 0.

In this study, precipitation was corrected by a nonlinear function of altitude taking account of varying

gradients and an eventual decrease at very high elevations. The correction factor f_c in Eq. (1) remains 1 over lower elevations for which observations are available, but increases exponentially up to a maximum gradient a (% m^{-1}). The gradient is then reduced until a maximum correction c (dimensionless) at altitude m (m MSL) is reached and decreases again at higher elevations thereafter:

$$f_c(z) = (c-1) \times \exp\left\{-\left[\frac{a}{(c-1)\times 100}\right]^2 \times (z-m)^2\right\} + 1. \quad (1)$$

This is a more continuous approach than the combination of two linear functions proposed by Immerzeel et al. (2012b). Parameter c is effectively the greatest correction applied, while the altitude m is the physical limit of the atmosphere to lose more moisture. For the Tien Shan, Aizen et al. (1995) described this exponential change in precipitation and provide valuable observations to constrain the parameters of the correction function for the multiobjective calibration. The investigations by Immerzeel et al. (2012b, 2015) helped to constrain the parameter ranges for the Karakoram region.

To account for local differences in precipitation underestimations across a catchment, the correction term c was distributed over selected glacier groups, totaling 6–11 in each catchment (Fig. S1 in the supplemental material). They were identified according to major glacier clusters at mountain massifs and their exposition. For subbasins without any glaciers, the values were interpolated between the groups using an inverse distance weighting (IDW) interpolation.

e. Model initialization, calibration, and validation

The model was calibrated using a multiobjective automatic optimization, considering observed discharge at the five outlet gauge stations, observed glacier area, and mass balances, where those were available. A calibration run consisted of the glacier initialization and a full hydrological run starting in the year with available discharge data (1964) and covering the reference period 1971–2000. The reference period was chosen because daily discharge data were available for the 1970s and 1980s for most stations (with some years missing, as listed in Table S1), and the geodetic mass balance analysis for the Aksu catchment by Pieczonka and Bolch (2015) is for the period 1975–2000. Following the split-sample calibration–validation approach, the available discharge data were split into 4-yr periods (the calendar years 1964–87, yielding six periods). The model was calibrated to all odd-numbered periods (1964–67, 1972–75, 1980–83) and validated to the even-numbered periods (1968–71, 1976–79, 1984–87). This method was preferred, because the day-to-day correlation of the precipitation data with discharge was found to be worse in the 1980s than in the 1970s (most likely caused by changes in meteorological station density). This meant that choosing either decade as the calibration or validation period would distort the results of the validation.

The calibration was supported by the recent findings of catchment-wide glacier mass balances for the Aksu catchments by Pieczonka and Bolch (2015). Since catchment-wide mass balances or representative local mass balance records for the Hotan and Yarkant catchments were not available, we used three initial mass balance scenarios and compared those to regional research findings (e.g., Holzer et al. 2015), as well as accounting for those scenarios in the uncertainty analysis. The initialization and calibration steps are further described below, and all calibration parameters with their ranges are provided in Table 3.

Glacier dynamics models need to be initialized over typical equilibrium time frames (200–1000 years) in order to ensure consistency between driving data, model structure, and ice cover (Marshall et al. 2011; Clarke et al. 2015). We initialized the SWIM-G model over 300 years and compared the resultant glacier cover to the observed glacier inventory. The fit of the ice hypsometry in each catchment was used to match the initialized glacier area to the observed, through the calibration of all parameters affecting the glaciers. It is quantified through the χ^2 objective function for histogram comparison between the two hypsometries as follows:

$$\chi^2 = \sum \frac{(A_{s,i} - A_{o,i})^2}{A_{s,i} + A_{o,i}} \times 100, \quad (2)$$

with observed A_o and simulated A_s glacier area for the 50-m elevation band i, expressed as percent. It ensures good fit also at the tail ends of the hypsometries due to the sum of observed and simulated areas in the denominator. The χ^2 is calculated for each glacier group of the catchment and weighted by the observed glacier area.

The initialization requires a climate period with known, quasi-stable mass balance conditions that is representative for the observed glacier cover. Although glaciers are never in a perfect equilibrium state, glaciers are globally identified as having stable conditions between the 1960s and the mid-1970s (Dyurgerov 2010). This is also true for the Tien Shan (Sorg et al. 2012; Farinotti et al. 2015). However, historic observations are limited for Kunlun Shan and Karakoram. Recent findings based on declassified satellite imagery indicate that glaciers in the Karakoram have been stable or showed only slight mass loss since the 1970s until today (Bolch et al. 2017;

TABLE 3. Calibration parameters and ranges used for the multiobjective calibration. Where different ranges were used, they are differentiated for either the Aksu or the Hotan and Yarkant catchments.

	Parameter/description	Range	Unit
	Precipitation		
c	Maximum correction factor	1–6[a] 1–15[b]	
a	Maximum precipitation gradient	0.1–0.9	% m^{-1}
m	Maximum precipitation altitude	4000–7000	m MSL
	Snow and glaciers		
δ_s	Snow degree-day factor	2–7[a] 1–5[b]	mm $°C^{-1}$ day^{-1}
T_m	Snowmelt threshold temperature	0 ± 3	°C
t_e	Temperature lapse rate	−0.80 to −0.55	°C $(100\,m)^{-1}$
δ_g	Ice degree-day factor	6–14[a] 2.5–7[b]	mm $°C^{-1}$ day^{-1}
Γ	Proportion of energy consumed by sublimation	0.2–0.6[a] 0.4–0.9[b]	
b_r	Residual mass balance during initialization	0 ± 0.34[a] −0.1, 0, +0.1[b]	m w.e. a^{-1}
	Hydrology		
E_c	Potential evaporation correction	0.7–1.3	
$R_{2,4}$	Routing coefficients	1–20	
S_c	Saturated conductivity correction	0.1–2	

[a] Aksu catchments
[b] Hotan and Yarkant catchments

Zhou et al. 2017). Dyurgerov (2010) provides "best guess" regional glacier mass balances since the 1960s for all major glacier regions. For the initialization period between 1960 and 1975, mean mass balances of −82 mm water equivalent (w.e.) a^{-1} are given for the Tian Shan, −37 mm w.e. a^{-1} for the Tibetan Plateau, 176 mm w.e. a^{-1} for the Karakoram, and −52 mm w.e. a^{-1} for the Pamir. While these values should be used as guidelines only, as they mostly originate from single glaciers, they show mass balances less negative than the global mean of −330 mm w.e. a^{-1} in the period 1976–2005 (Zemp et al. 2009). This imbalance was corrected by a residual mass balance parameter during the initialization as was previously done by Clarke et al. (2015). A negative mass balance means ice is evenly added to all glacier surfaces at the end of the year and vice versa for a positive mass balance. Although this parameter is only used in the initialization run, it has a great impact on the mass balance simulations, as it changes the imbalance of the glacier cover at the beginning of the simulation. The residual mass balance was calibrated in the Aksu catchment, where mass balances estimates exist, and prescribed in a scenario approach in the Hotan and Yarkant catchment where they are absent.

Pieczonka and Bolch (2015) provide a catchment-wide mean mass balance including uncertainty range for the Xiehela (Aksu) catchment for the period 1975–2000. Because of their proximity and topographical similarities, we used these average values also in the neighboring Shaliguilanke catchment. The objective function for the automatic calibration assigned a score between 1 (worst) and 0 (exact match) based on the normal distribution probability function using the mass balance (MB) as the mean value and the uncertainty range as the standard deviation. It is defined as follows:

$$\mathrm{MB}_{\varepsilon} = 1 - \exp\left[-\frac{(\overline{b_s} - \overline{b_o})^2}{\varepsilon^2}\right], \tag{3}$$

where $\overline{b_o}$ is the mean annual mass balance over the study period by Pieczonka and Bolch (2015) (0.35 m w.e. a^{-1}) with an uncertainty range of ε (= 0.34 m w.e. a^{-1}) and the simulated mass balance $\overline{b_s}$ over the same period. In the Hotan and Yarkant catchments, representative mass balance records are absent, but some regional indications and recent findings exist (they are discussed in section 4). We therefore calibrated these catchments for three initial mass balance scenarios of +0.1, 0, −0.1 m w.e. a^{-1}, with the simulated mass balances discussed in the results. These values are guided by the best-guess values mentioned above. The 0.1 m w.e. a^{-1} max/min values represent about 30% of the expected catchment precipitation and nearly twice as much as is recorded in the APHRODITE data. A mass balance outside of that range would mean a strong glacier imbalance that has not been observed elsewhere in High Asia during the 1960s and 1970s and is thus considered unlikely.

In addition to the simulated glacier dynamics, the catchment hydrology was calibrated to the available discharge records from the five outlet gauge stations (Table 1). The hydrological performance was measured by one objective function for the daily discharge and a second objective function for annual discharge. The first objective function applied to daily discharge is a combination of the standard and logarithmic Nash–Sutcliffe efficiency (NSE; Nash and Sutcliffe 1970). Because of the strong seasonality in the catchments, the inclusion of the logarithmic NSE prevents the strong summer peaks from receiving the greatest weight in the common NSE measure, as was observed by Duethmann et al. (2014, 2015). The objective function is given by the following equation:

$$\mathrm{NSE}_c = \frac{1}{2}\left[2 - \frac{\sum(Q_s - Q_o)^2}{\sum(Q_o - \overline{Q_o})^2} - \frac{\sum(\log Q_s - \log Q_o)^2}{\sum(\log Q_o - \log \overline{Q_o})^2}\right], \tag{4}$$

with observed Q_o and simulated Q_s daily mean discharge and the observed long-term average $\overline{Q_o}$. For the model validation, this objective function was also evaluated for the validation years (odd-numbered periods).

A second objective function using the annual discharge was used to also optimize the model to the annual water balance and the interannual variability. This was done through a simple root-mean-square function as described by

$$\mathrm{RMSE}_{\mathrm{QA}} = \frac{\sqrt{(\mathrm{QA}_s - \mathrm{QA}_o)^2}}{\overline{\mathrm{QA}_o}} \times 100, \tag{5}$$

with squared residuals between observed QA_o and simulated QA_s annual mean discharge weighted by the observed long-term average discharge $\overline{\mathrm{QA}_o}$ expressed in percent.

We employed the S-metric selection evolutionary multiobjective optimization algorithm (SMS-EMOA) to optimize the four objective functions using the 12 calibration parameters listed in Table 3. The algorithm successively finds Pareto optimal solutions out of a parameter set population of 100 ''individuals'' by optimizing the hypervolume enclosing the space of dominated (not Pareto optimal) solutions (Beume et al. 2007; Emmerich et al. 2005). Its advantage over other commonly used multiobjective optimization algorithms [e.g., Nondominated Sorting Genetic Algorithm (NSGA-II)] is the preference of solutions well-spaced out on the Pareto front, rather than clustering many solutions over smaller parts of the front. It has been used successfully in hydrological modeling studies with similar multicriteria problems (Ficklin et al. 2014; Stagge and Moglen 2014).

The model was optimized for each of the five catchments individually and run for a population of 100 in parallel on a large computer cluster over 100 generations. Satisfactory convergence results were already attained after 50–70 generations, that is, 5000–7000 model runs. The remaining ''Pareto optimal'' solutions were inspected and the following minimum criteria were defined: 1) an NSE_c of at least 0.6, 2) an $\mathrm{RMSE}_{\mathrm{QA}}$ less than 25%, 3) a χ^2 less than 20%, and 4) an MB_ε error probability of lower than 0.05 (only in the Aksu catchments). These criteria were used to filter out solutions at the edges of the Pareto front. The remaining count out of 100 will be reported in the results along with median values over all remaining ones.

3. Results

a. Comparison of precipitation datasets

Mean annual precipitation varies widely between the selected datasets in both space and time. The discrepancies are evident in catchment mean values (Table 4) and mean annual and monthly values (Fig. 3, Fig. S2), as well as horizontal (Fig. 4) and vertical distributions of precipitation (Fig. 5). Some datasets refer to different periods than 1971–2000 (our reference period); these periods are clearly indicated in the figures, where they are shown together. Although care must be taken when comparing values of different periods, the annual variability is below the differences between most of the precipitation datasets (Fig. 3). As described in section 2b, we are referring to the three categories of datasets as direct, satellite-based, and model-based precipitation datasets (DPD, SPD, MPD).

In the Aksu catchments (Xiehela and Shaliguilanke), the DPD show mean annual values of 230–320 mm a^{-1}, while ERA-Interim and CCLM are higher at 482–838 mm a^{-1} over the reference period (Table 4). These differences are also reflected in much higher summer precipitation for ERA-Interim and CCLM compared to the DPD and higher precipitation at higher altitudes for HAR, ERA-Interim, and CCLM (Fig. 5, Fig. S2). Although slightly lower, the DPD are in line with observations from the single high-altitude Tian Shan meteorological station (≈3600 m MSL), ranging between 200 and 400 mm a^{-1}. However, the altitude dependence is only vaguely visible, with most of the Tian Shan showing values between 200 and 300 mm a^{-1}. At similar spatial resolutions, ERA-Interim, HAR, and CCLM show much higher values, especially at the north eastern fringe of the Xiehela catchment.

TABLE 4. Catchment mean annual precipitation ± standard deviation over the catchment area. Means and standard deviations over 1971–2000 unless otherwise stated.

	Aksu		Hotan		Yarkant
	Xiehela	Shaliguilanke	Wuluwati	Tongguziluoke	Kaqun
APHRODITE	314 ± 63	230 ± 20	98 ± 28	62 ± 11	113 ± 24
GPCC	320 ± 90	238 ± 25	63 ± 27	44 ± 3	111 ± 39
TMPA (1998–2015)	390 ± 83	300 ± 26	147 ± 38	148 ± 44	211 ± 54
ERA-Interim (1979–2000)	838 ± 123	486 ± 80	566 ± 137	572 ± 138	566 ± 195
CCLM	617 ± 150	482 ± 160	548 ± 167	567 ± 160	609 ± 134
HAR (2001–2014)	1213 ± 499	894 ± 253	276 ± 137	439 ± 232	463 ± 388

In the Hotan and Yarkant catchments, catchment mean values of the DPD are in the range of 44–113 mm a^{-1}, values similar to the Taklamakan Desert. The region's typical summer precipitation peak is not evident in the Wuluwati and Kaqun catchments, while there is virtually no precipitation recorded between October and March in the Tongguziluoke catchment (see Fig. S2). This leads us to conclude that the DPD are strongly biased by the observations in the desert with annual mean values below 100 mm a^{-1} in the Hotan and around 100–150 mm a^{-1} in the Yarkant catchment. The SPD and MPD, on the other hand, have mean values of 147–609 mm a^{-1} and show a greater correlation with the major mountain ranges in the region. The high-resolution GPM and HAR datasets show the heterogeneities in precipitation well. For example, in the HAR dataset, the strong differences between the north of the Yarkant catchment and the much wetter Karakoram in the south are striking (Fig. 4). This elevational dependence in precipitation over the catchments is barely noticeable in the DPD (Fig. 5).

A first-order indication of precipitation underestimation is also provided by runoff coefficients, the ratio of catchment discharge to precipitation. For four of the five catchments, runoff coefficients are greater than 1 with precipitation from the DPD (Table 5). The Hotan and Yarkant catchments have exceptionally high coefficients above 1 and up to 3.9. Runoff ratios for the ERA-Interim and CCLM precipitation, on the other hand, are much lower at 0.19–0.60. Coefficients roughly vary with glacier cover and aridity, with the highly glacierized catchments Xiehela and Tongguziluoke showing significantly higher values than their neighboring less glacierized catchments, Shaliguilanke and Wuluwati.

The extensive glacier cover of the catchments has the potential to alter runoff without a change in precipitation due to its dependence on temperature. Negative mass balances drive the ratio up and vice versa, but only within the limits of reasonable mass balance assumptions. Simultaneously, mountainous catchments generally exhibit high runoff coefficients, as the existence of permafrost, shallow soils, and steep slopes favor fast surface runoff and low temperatures coupled with sparse vegetation keep evapotranspiration low (Goel 2011). However, in the Tarim headwaters this is counterbalanced by an arid to hyperarid climate. Numerous high-altitude saltwater (endorheic) lakes are close to the catchments on the Tibetan Plateau and in the western central Tien Shan (e.g., Aksai Chin Lake, Chatyr Kol), providing evidence for evaporation-driven water cycles. These opposing conditions and uncertain mass balances in the Yarkant and Hotan catchments for this period make it difficult to estimate reasonable runoff coefficients. But even with—for the region, atypically large—negative mass balances (i.e., from −500 to −600 mm w.e. a^{-1}), coefficients greater than 1 are improbable and would signal a significant alteration of the glacier and catchment hydrology.

In summary, the comparison of the six precipitation datasets in the Tarim headwater catchments revealed the following:

1) The SPD and MPD give significantly higher values than the DPD (catchment means 3–4 times higher, locally up to 12 times).
2) The mountain ranges are not well reproduced by the DPD, especially where the closest meteorological stations are at the desert fringes.
3) The DPD do not capture the heterogeneity and elevation dependence of precipitation in the catchment as it is, for example, measured by the satellite-based datasets or modeled by the MPD.
4) All datasets vary significantly from each other, especially in the elevation distribution, with the exception of the strong similarity between the DPD.

To reconcile these differences into a consistent and, for modeling purposes, useful precipitation dataset, we correct the daily APHRODITE dataset. Despite its weaknesses at higher elevations, it is the only daily dataset available for many decades, it has the greatest meteorological station density, and it shows a strong correlation with the observed discharge, in comparison to the climate

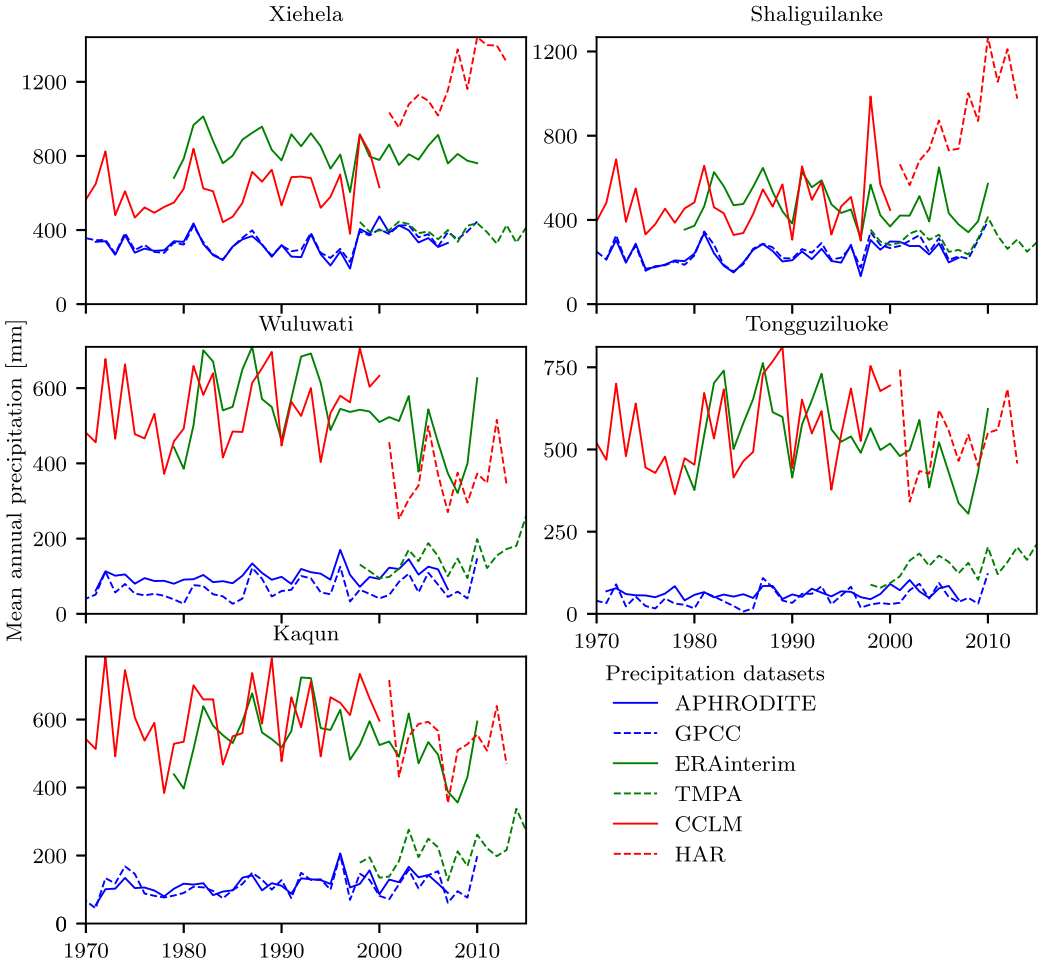

FIG. 3. Annual mean precipitation for the selected datasets (1971–2015): (top) the Aksu catchments, (middle) the Hotan catchments, and (bottom) the Yarkant catchment (titles are the station names). Note the varying vertical scales.

model-based datasets. But using the findings of the above comparison allowed us to constrain the correction with the help of the glacio-hydrological model SWIM-G.

b. *Model calibration*

The automatic calibration of the SWIM-G yielded good results, but performances vary with meteorological station density (Table 6). The population size of 100 parameter sets was subset using acceptable threshold values (see section 2e and top of Table 6) for the four objective functions (NSE, RMSE of annual discharge, χ^2 of glacier hypsometry, and MB). The subsets include all of the runs in the Xiehela (Aksu) catchment, 49 runs for the Shaliguilanke (Aksu catchment), 51–83 in the Hotan catchments, and 84–97 in the Yarkant catchment. The results for the Hotan and Yarkant catchments are given with uncertainty ranges over the three mass balance assumptions in the initialization period. Calibrated parameter values are listed in Tables S2–S4 in the supplemental material.

The glaciological calibration is mainly characterized by the match between the observed and simulated (initialized) ice hypsometries (Fig. 6), evaluated by the objective function χ^2. The overall hypsometry is generally in good agreement with the observed one, with median χ^2 deviations of 4.0%–14.7%. Departures from the observations mainly occur at overestimated hypsomety peaks, as a result of the χ^2 objective function that weighs errors relative to the observed magnitude, compromising overestimations in the peaks against better fits at the lower ends. Differences between the initial mass balance assumptions for the Hotan and Yarkant catchments are small (0.6%–1.3% in the median χ^2), giving evidence that the precipitation correction has compensated for the loss/gain in ice for positive/negative mass balances in the initialization period.

The hydrological calibration, gauged by the combined NSE and the RMSE of annual mean discharge, yielded good results, but differences with meteorological station

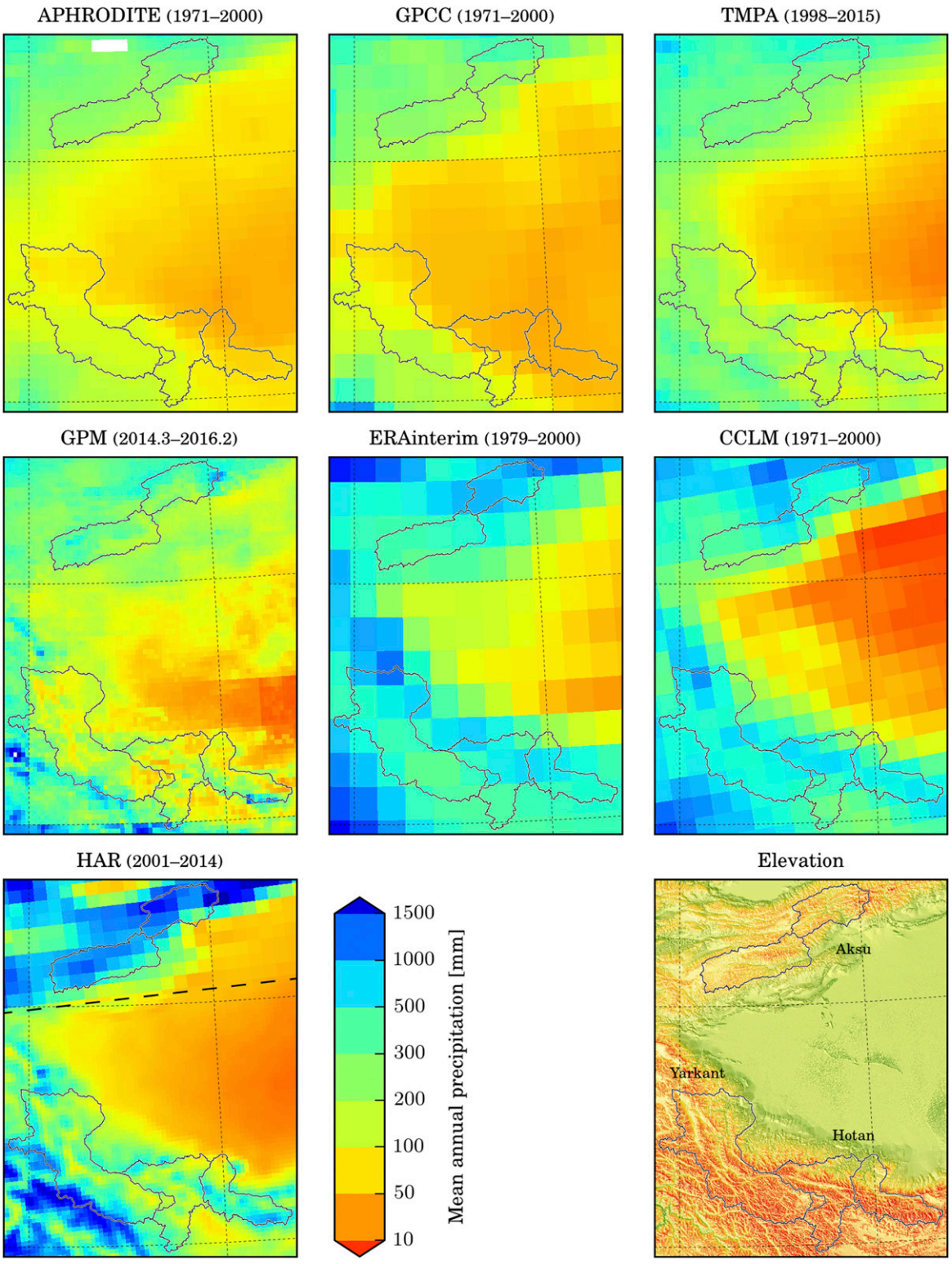

FIG. 4. Mean annual precipitation for the selected datasets over the periods stated in the title. The APHRODITE, GPCC, and CCLM datasets all refer to the reference period 1971–2000. All datasets are shown at their original resolution but in UTM projection. Elevation from the SRTMv3 DEM for reference; refer to Fig. 1 for elevations and scales. The horizontal line in the HAR dataset indicates the boundary of the 10-km-resolution domain; the northern part is the 30-km-resolution domain. Note the nonlinear color scaling.

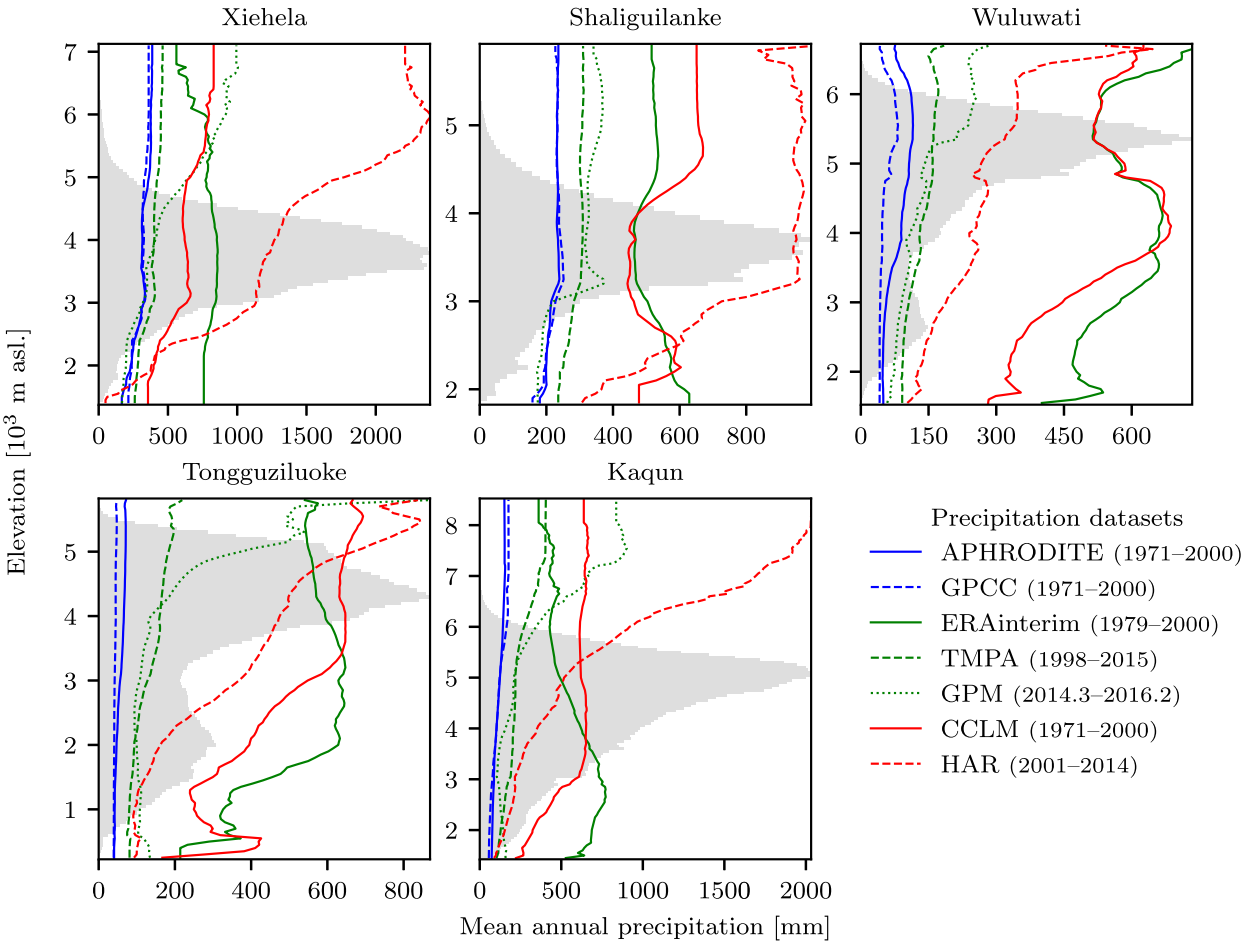

FIG. 5. Mean annual precipitation (1971–2000, unless otherwise stated) hypsometries over the five headwater catchments. The 50-m elevation intervals are sampled from the original values at a horizontal 90-m resolution. The shaded area indicates the catchment hypsometry.

densities are apparent (Fig. 7). Whereas the two Aksu catchments and the Yarkant catchment have NSE_c values of above 0.82 and an annual discharge error of less than 16%, these objective functions decline to around 0.74% and 21% in the Hotan catchments. The validation NSE_c value is 0.035–0.045 lower than the calibration value. The day-to-day variability as well as the day of year mean seasonality are reproduced well, but the erratic discharge peaks in summer are often missed by the simulations, especially in the Hotan catchments. The range in discharge over the calibration ensemble is relatively small but is usually greatest in autumn, with some exceptions in the Yarkant catchment. While catchment discharge was used for the automatic calibration, it is only one component of the catchment hydrology. Results of the other components (snowmelt, evapotranspiration, etc.) will be presented in the next section and should also be considered in the model calibration and its hydrological plausibility. Most discharge

TABLE 5. Runoff coefficients for the datasets with overlap with discharge observations (1971–87).

	Aksu		Hotan		Yarkant
	Xiehela	Shaliguilanke	Wuluwati	Tongguziluoke	Kaqun
APHRODITE	1.10	0.62	1.26	2.51	1.38
GPCC	1.08	0.61	1.99	3.87	1.39
ERA-Interim	0.43	0.30	0.19	0.26	0.25
CCLM	0.60	0.31	0.22	0.29	0.25

TABLE 6. Model performance according to the median values of the four objective functions over the calibration ensemble (NSE_c, $RMSE_{QA}$, χ^2, and MB_ε). By applying the thresholds shown in the table header, the 100 Pareto-optimal calibrations are reduced to number N. The NSE_c is given for the calibration (even years) and the validation years (odd years). In the Hotan and Yarkant catchments, mean values are provided for three mass balance assumptions (b_r = +0.1, 0, −0.1 m w.e. a^{-1}), instead of MB_ε.

		N	NSE_c		$RMSE_{QA}$ (%)	χ^2 (%)	MB_ε
			Calibration	Validation			
Threshold			0.60		25.0	20.0	0.05
Aksu							
Xiehela		100	0.936	0.889	13.4	8.4	0.001
Shaliguilanke		49	0.827	0.787	16.3	14.7	0.023
Hotan	b_r						
Wuluwati	+0.1	51	0.739	0.701	20.8	11.5	
	0	73	0.739	0.700	20.9	10.9	
	−0.1	67	0.734	0.696	20.1	11.8	
Tongguziluoke	+0.1	75	0.704	0.669	23.0	4.8	
	0	83	0.742	0.706	21.9	4.1	
	−0.1	83	0.765	0.728	21.1	4.0	
Yarkant	b_r						
Kaqun	+0.1	93	0.827	0.785	16.9	9.8	
	0	84	0.827	0.786	15.8	10.2	
	−0.1	97	0.856	0.813	16.6	11.1	

is generated by surface runoff (in the Aksu catchments) or interflow (Hotan and Yarkant catchments), while groundwater contributes about a third of total annual runoff (Fig. S3).

The simulated glacier mass balance in the two Aksu catchments was accurately calibrated to the catchment-wide values found by Pieczonka and Bolch (2015) for the period 1975–2000 (Fig. 8, top). While the simulated annual variability is close to the in situ mass balance record at Karabatkak Glacier (scaled in Fig. 8, top), it is more positive in the early 1980s and slightly more negative in the late 1990s. The calibration ensemble range (−0.35 ± 0.06 m w.e. a^{-1}) is lower than the accumulated uncertainty found by Pieczonka and Bolch (2015) (−0.35 ± 0.34 m w.e. a^{-1}). Mass balance is mainly calibrated via snow and ice degree-day melt rates as well as the residual mass balance during initialization. The calibrated residual mass balance median (± standard deviation) is −0.19 ± 0.02 m w.e. a^{-1}

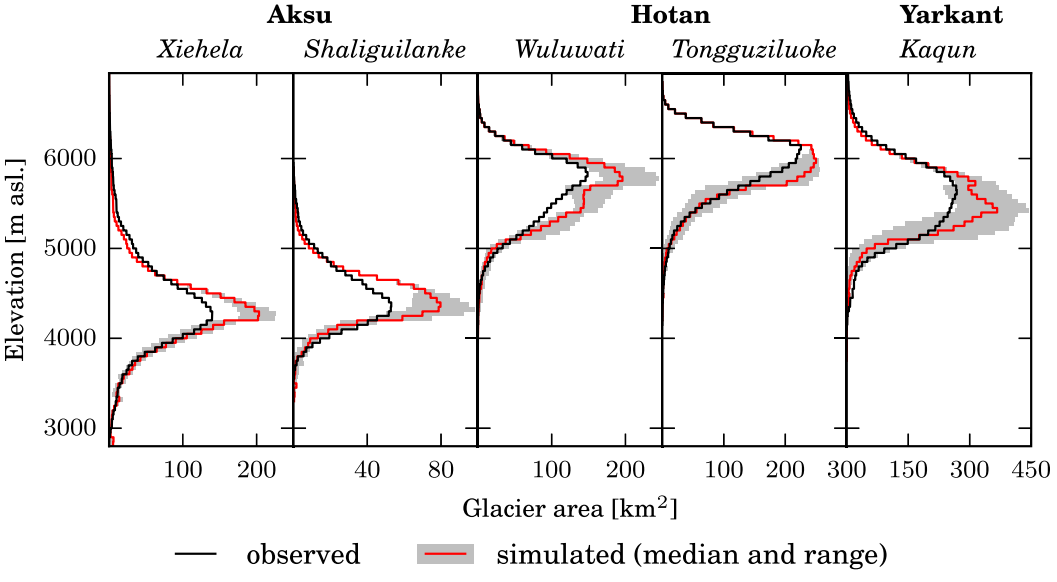

FIG. 6. Initialized and observed glacier hypsometry of the five headwater catchments. Hypsometry intervals are 50 m. Note the variable horizontal scales.

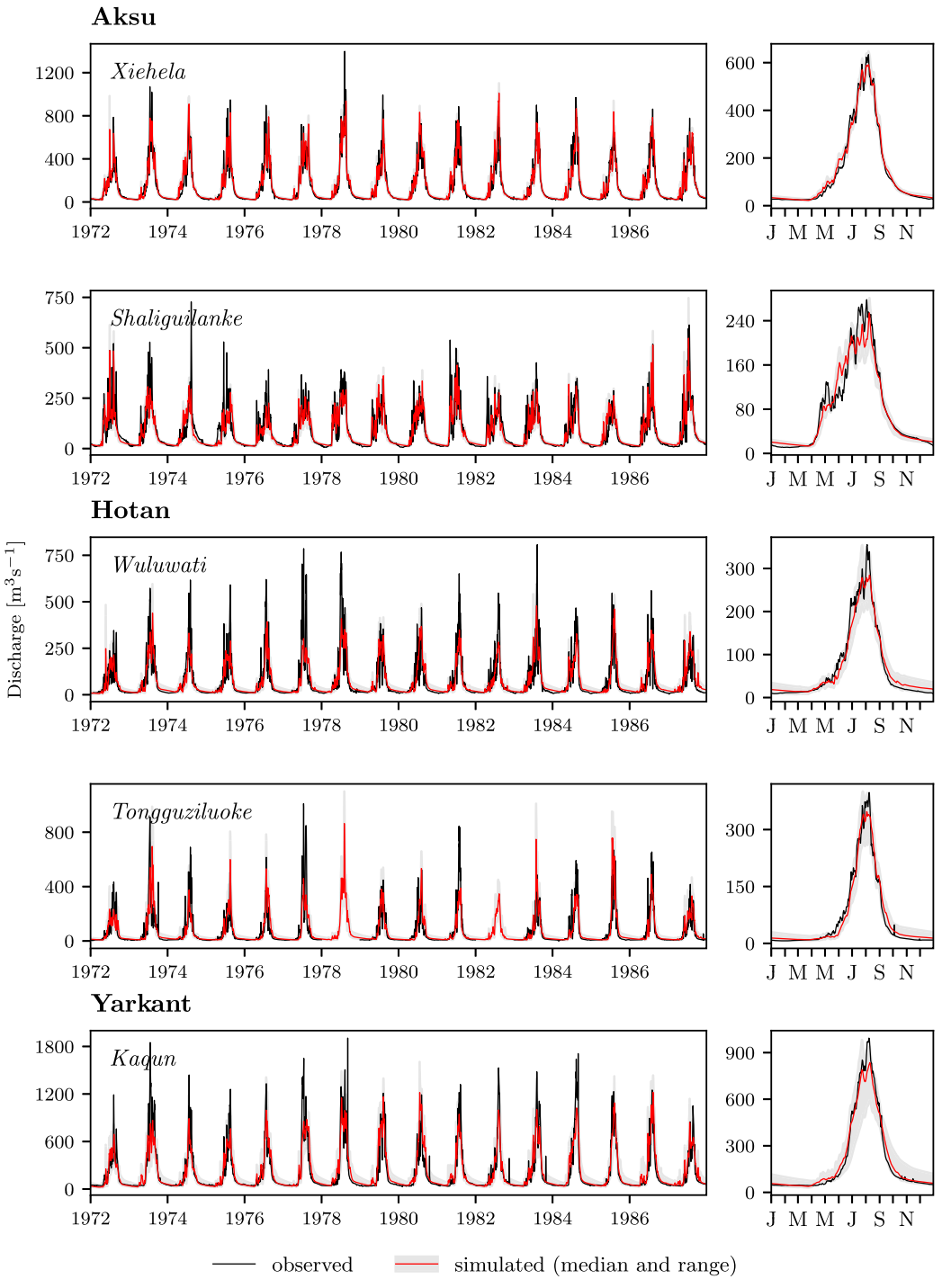

FIG. 7. Simulated and observed daily and day-of-year mean discharge for all five gauging stations over the last two calibration (1972–75, 1980–83) and last two validation (1976–79, 1984–87) periods. Observation data were available for 4–7 additional years outside of the shown period, which was chosen for clarity and the greatest overlap of available discharge data.

for the Xiehela catchment and -0.16 ± 0.04 m w.e. a^{-1} for the Shaliguilanke catchment, which is within the values found in a modeling study for the Tien Shan for the same period (Farinotti et al. 2015).

The simulated mass balances in the Hotan and Yarkant catchments are stable or increasing under all three initial mass balance assumptions (Fig. 8, bottom two panels). Increasing with the residual mass balance assumption,

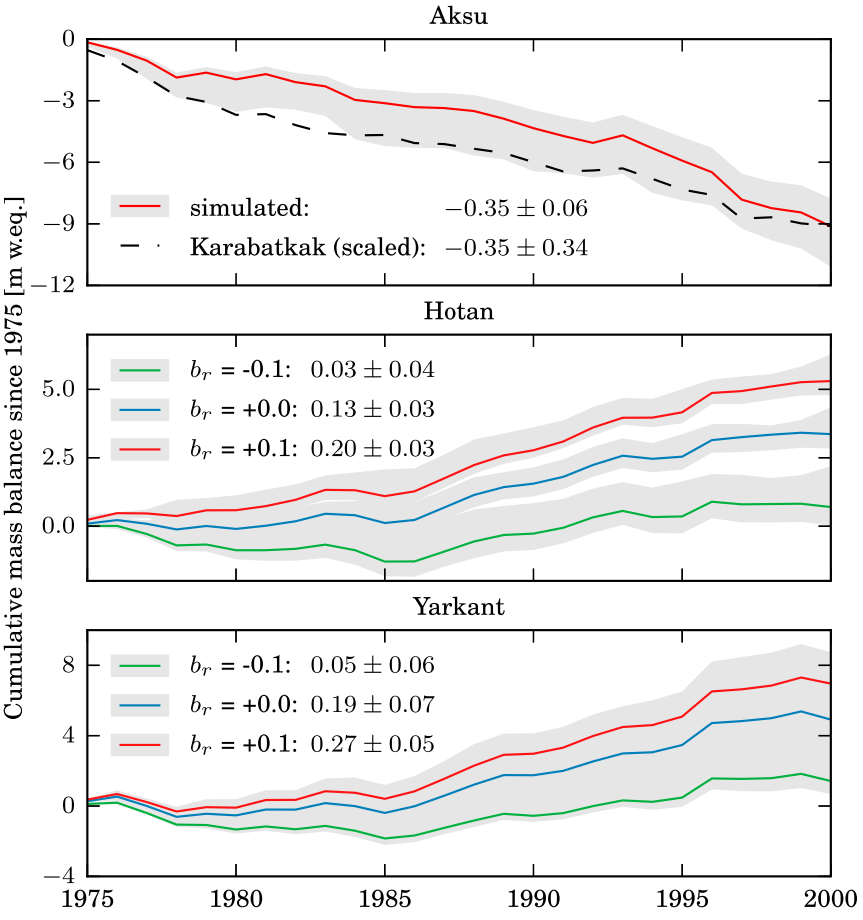

FIG. 8. Simulated mass balance in the period investigated by Pieczonka and Bolch (2015) with median and min/max ranges drawn and annual mean values (m w.e. a^{-1}) with uncertainties (half-range over all runs) given in the legend. The Karabatkak mass balance is scaled to the catchment-wide mean value found by Pieczonka and Bolch (2015) for the Aksu catchments. As observations for the Hotan and Yarkant catchments do not exist, the outcomes of the three initializations with different mass balance assumptions are shown.

median values range between 0.03 and 0.20 m w.e. a^{-1} in the Hotan and between 0.05 and 0.27 m w.e. a^{-1} in the Yarkant catchment, with uncertainty ranges (half-range over all runs) of 0.03–0.07 m w.e. a^{-1}. The annual variability is similar in those catchments; it is stable to slightly negative between 1975 and 1985 and increasing thereafter. These simulations are in line with several, mostly local, glaciological studies from the Kunlun Shan and the Karakoram, as is discussed in more detail in section 4. The increasing trend, even with a negative initialization mass balance, is driven by increases in precipitation in comparison to the initialization period (1961–75), while temperature changes are moderate.

c. *Corrected precipitation*

Corrected catchment mean precipitation as well as other water balance components are shown in Fig. 9 and the distribution of mean annual precipitation over the five catchments in Fig. 10. The simulated precipitation is far higher than the APHRODITE dataset suggests: at the catchment average by a factor of about 1.5 in the Aksu catchments, 2.2 in the Wuluwati (Hotan) and the Kaqun (Yarkant) catchments, and by a factor of about 4.3 in the Tongguziluoke (Hotan) catchment (Fig. 11). In the calibration ensemble median, the highly glacierized Xiehela (Aksu) catchment receives 487 mm a^{-1} (corrected from 314 mm a^{-1}) on average over the reference period 1971–2000 and the less glacierized, lower-lying Shaliguilanke (Aksu) catchment to the southwest receives 327 mm a^{-1} (corrected from 230 mm a^{-1}). Correction factors over the large massifs, the Kokshal–Too in the west and the Inylcheck–Tomur regions, are between 2 and 5 with precipitation totals of up to 1400 mm a^{-1}. The two Hotan catchments south of the Taklamakan Desert were strongly corrected due to the

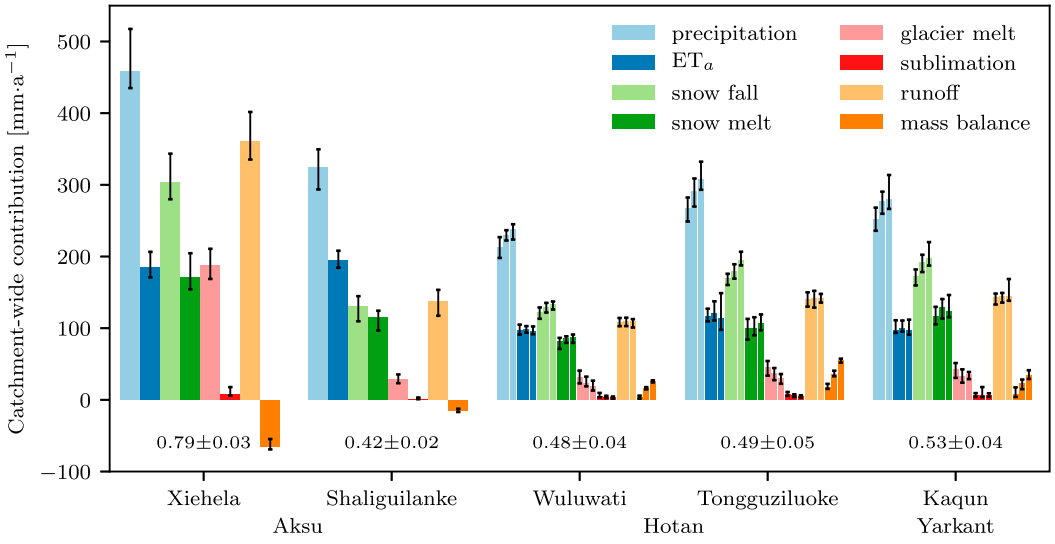

FIG. 9. Simulated water balance components averaged over all five catchments, median (solid bars), and ensemble min and max (error lines). The three initial glacier mass balance assumptions for the Hotan and Yarkant catchments are indicated by divided bars and three error lines for those catchments (from left to right: MB = −0.1, 0.0, +0.1 m w.e. a^{-1}). The corresponding runoff coefficients (median ± half-range) are given as numbers for each catchment. The sublimation is only from glaciers as sublimation from snow is not modeled explicitly.

absence of any meteorological station to 285 mm a^{-1} (from 62 mm a^{-1}) in the highly glacierized Tongguziluoke catchment and 230 mm a^{-1} (corrected from 98 mm a^{-1}) in the drier Wuluwati catchment with large parts on the Tibetan Plateau. The West Kunlun Shan massif in the southwest of Tongguziluoke catchment requires factors of 5–10 to sustain its vast glacier cover. The precipitation patterns are more heterogeneous in the much larger Yarkant catchment; the catchment-wide average was corrected to 267 mm a^{-1} (from 113 mm a^{-1}). The Karakoram in the south of the catchment, however, receives a range of 500–1200 mm a^{-1}, much more than the rest of the catchment, with high correction factors of 5–9.

It is apparent that regions with very large correction factors (i.e., >5) are also very far away from any meteorological station (Fig. 2), both horizontally and vertically. For example, the West Kunlun Shan massif and the northeastern Karakoram are 50–100 km away from the nearest precipitation gauge as well as several thousand meters higher. The large correction factors clearly stem from entirely different precipitation regimes and not only orographic precipitation. In the Aksu catchments, on the other hand, meteorological stations are closer but mainly located at lower altitudes, leading to lower correction factors that mainly correspond to orographic precipitation.

The simulated runoff coefficients are more reasonable than those calculated with the DPD (Fig. 9). Evaporation ranges between 100 and 200 mm a^{-1}, comparing well with global modeling results (Table S5). Low relative humidity, high elevations, and windy conditions favor sublimation, consuming large proportions of a glacier's energy balance, as studies from tropical glaciers have shown (Winkler et al. 2009; Gascoin et al. 2011). In comparison to glacier melt, however, sublimation from glaciers is a relatively small factor in the catchments' water balance because it consumes approximately 8.5 times more energy than melting (Mölg et al. 2009). The fraction of energy consumed by sublimation was calibrated to 0.2–0.3 in the Aksu catchments and 0.5–0.6 in the drier Hotan and Yarkant catchments.

We use the coefficient of variation (standard deviation as percent of mean) over the calibration ensemble to describe the spatial pattern of the uncertainty, referred to as just uncertainty hereafter (Fig. 12). Since the mass balance of the Aksu catchments is calibrated, the uncertainty is at around 10%–20% smaller than in the Hotan and Yarkant catchments, where most parts have uncertainties of about 20% and in some locations of up to 45%. The mean catchment uncertainty, however, is much smaller at 5%–7% in the Aksu catchments and 12%–15% in the Hotan and Yarkant catchments. Uncertainties are generally greater at higher altitudes, where they are mainly distributed according to the glacier area that the calibration to ice hypsometry depends on. The highly glacierized areas mostly have the highest correction factors but also lower uncertainties than other high-altitude parts of the catchment. These latter areas typically have small glaciers covering only small

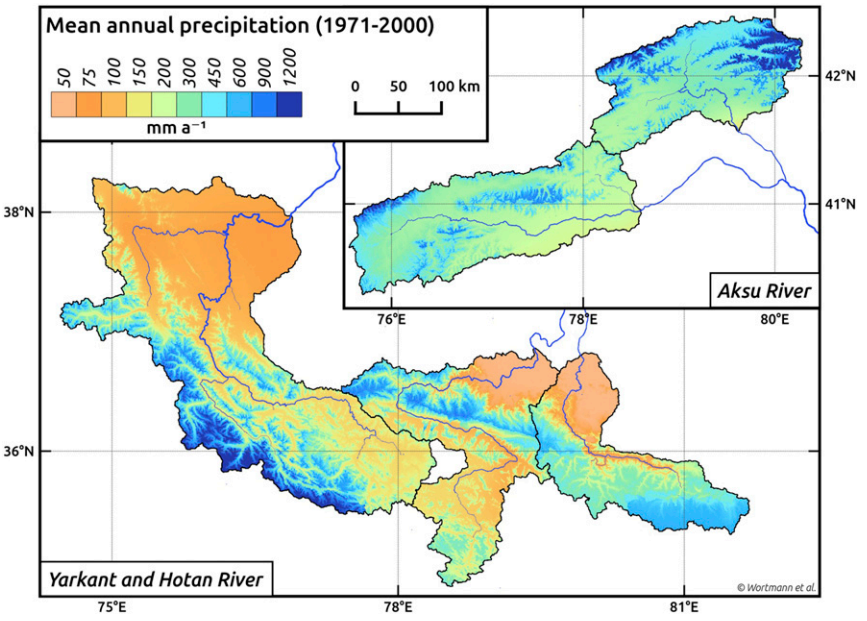

FIG. 10. Corrected mean annual precipitation (1971–2000) over the five catchments, based on the APHRODITE reanalysis dataset. Modeled hydrotope/glacier unit values are given at a 90-m spatial resolution. The nonlinear color bar indicates lower boundaries.

parts of the terrain's hypsometry. The parameters of the precipitation correction are free to vary more than in areas where glaciers cover larger parts of the altitude range. For example, the precipitation estimations in the central east of the Wuluwati (Hotan) and the southeast of the Yarkant catchment with uncertainty values of around 40% are based on a relatively small glacier group with predominantly smaller glaciers.

In comparison to the six selected precipitation datasets, the corrected values fall between the SPD and the MPD. In the Aksu catchments, they are closest to the TMPA and CCLM catchment averages, and in the Hotan and

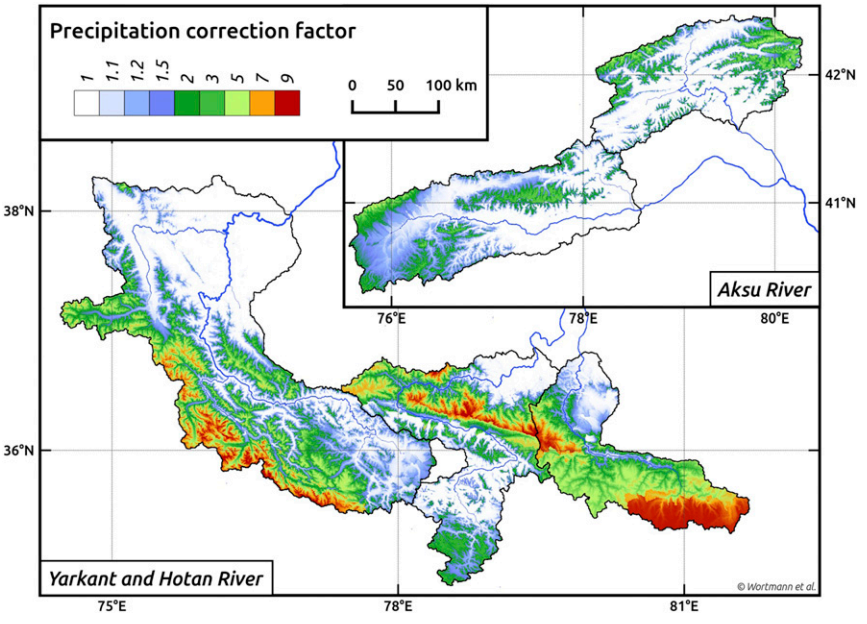

FIG. 11. Ensemble median precipitation correction factors for the APHRODITE reanalysis dataset (1971–2000). Hydrotope/glacier unit values at 90-m spatial resolution. The nonlinear color bar indicates lower boundaries.

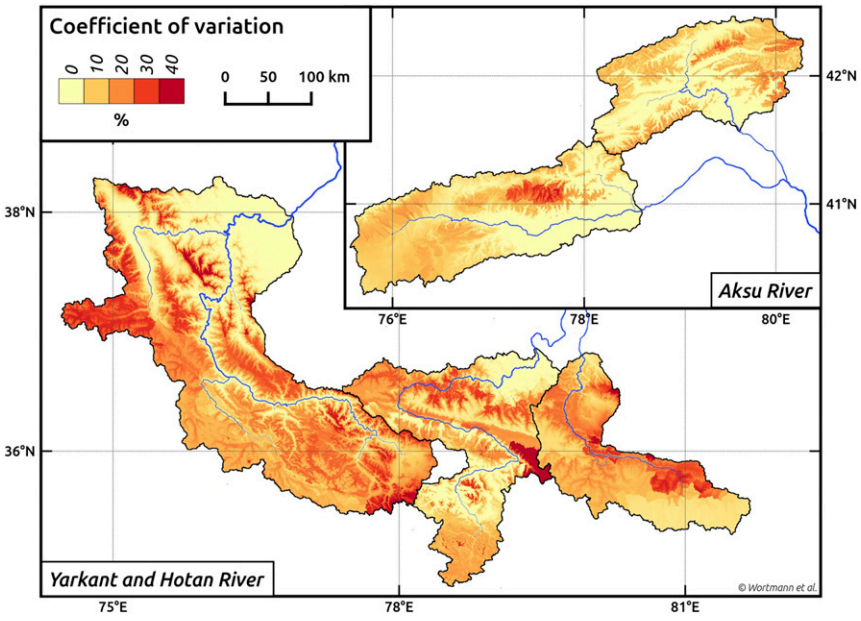

FIG. 12. Coefficient of variation over the calibration ensemble over all five catchments (hydrotope/glacier unit values at 90-m spatial resolution). The color bar indicates lower boundaries.

Yarkant catchment they are between the TMPA and HAR values. The spatial distribution of the corrected precipitation corresponds closer to higher-resolution datasets than the original APHRODITE data does (cf. Fig. 4 and Fig. 10), that is, the HAR dataset in particular. At the catchment average, the two SPD and MPD covering the simulation period, CCLM and ERA-Interim (only from 1979), show larger values with catchment means greater by a factor of 1.2–2.1 and 1.5–2.3, respectively. Although it is covering a different period, the high-resolution HAR dataset is closer in the Hotan and Yarkant catchment with deviations of 1.2–1.5 times greater. The precipitation patterns around the large massifs are similar to the high-resolution HAR and the GPM datasets. Although they are only available for more recent periods, they provide evidence for high orographic precipitation of up to 1000–1500 mm a^{-1}, for example, on the northern ridge of the Karakoram or at the crests of the Kunlun Shan, corroborating the large correction factors found with our simulations. Our corrected values, however, deviate from most other SPD and MPD in the north of the Yarkant catchment: corrected values range between 80 and 200 mm a^{-1}, but most SPD and MPD indicate higher values of around 200–500 mm a^{-1}. This is also reflected in relatively high uncertainties (Fig. 12) that are probably a result of the contrast between sparse and relatively small glaciers in the north and an extensive glacier cover in the south in this vast catchment.

4. Discussion

a. *Uncertainties in precipitation datasets*

Strong precipitation underestimations and necessary corrections in remote mountainous regions associated with strong elevation gradients have been studied before, but not in the Tarim headwaters (You et al. 2012; Henn et al. 2016). Deficiencies in various reanalysis datasets were corrected in the Syr Darya headwaters in Kyrgyzstan using a hydrological model under data-scarce conditions (Duethmann et al. 2013). Also, observations from the better-gauged Alps confirm large gradients between valley and high altitudes, providing further evidence for the necessity for strong corrections in regions with a low elevation sampling bias (Frei and Schär 1998; Sevruk 1985). As the great variability between the selected datasets and the high simulated correction factors in our results show, the Tarim headwaters are another example of such deficiencies.

The comparison of the six precipitation datasets has exposed considerable disagreement. The DPDs seem to be ineffective in representing orographic precipitation, although some effort is made to give greater weight to observations on windward facing and higher-elevation slopes [e.g., Yatagai et al. (2012) use the Mountain Mapper approach]. However, they do not extrapolate into ungauged elevation ranges, leading to a low elevation–low precipitation bias. But station distribution may not be the only reason for bias, as

measurement errors such as undercatch lead to further underestimations (Kochendorfer et al. 2017; Yang and Ohata 2001). Strong winds and large shares of solid precipitation, as found in the Tarim headwaters, make the observations especially susceptible. A recent study of high-resolution datasets over the western United States has shown biases of 5%–60% in long-term mean annual precipitation in a region with a much denser observation network compared to the Tarim headwaters (Henn et al. 2018).

The precipitation correction presented here is able to overcome these biases by incorporating available hydrological and glaciological observations, bringing it closer to the satellite and model-based datasets. It is, however, lower than the coarser-resolution datasets, ERA-Interim (0.5°) and CCLM (0.44°) as well as HAR (30 km) in the Aksu catchments, agreeing with previous findings over the southeastern Tibetan Plateau (Tong et al. 2014). Runoff coefficients and the associated water balance components are more plausible with the corrected precipitation than those for the DPD (Fig. 9). For the arid yet highly mountainous catchments, the simulations result in runoff coefficients between 0.4 and 0.6. An exception is the relatively wet and highly glacierized Xiehela (Aksu) catchment, where higher runoff paired with a negative mass balance results in a median value of 0.76. As a result, glacier melt accounts for 40%–50% of river runoff in this catchment [as has been found before by Duethmann et al. (2015) and also by older Soviet literature as described in Sorg et al. (2012)]. In the other catchments it is between 25% and 35%.

Assessing the uncertainty of the simulated evapotranspiration in comparison to observations is difficult. Observations of evapotranspiration in mountainous regions are extremely scarce, and the same applies to the headwaters of the Tarim River. To our best knowledge there are no direct observations available. Remote sensing–based products are insufficient for mountainous regions as they rely on vegetation indices and are thus often not available for desert and mountainous regions. The most widely available MODIS-based product (MOD16; Mu et al. 2007) is not available for approximately 90% of our model domain. However, we compared our simulations to three global hydrological model runs (see Table S5) from an ensemble presented in Haddeland et al. (2011) and provide a parameter uncertainty range through the ensemble calibration approach. Our simulations compare well with simulations of the Global Water Availability Assessment (GWAVA) and the Max Planck Institute Hydrological Model (MPI-HM) when they are driven by reference runs of a global climate model (ECHAM5). The values fall within ±20% of the SWIM-G simulations. The MPI-HM model was also driven by the EU Water and Global Change (WATCH) reanalysis data, which is based on the GPCC precipitation data also analyzed here. Although slightly lower, the results are comparable in the Aksu catchments (−7%) and are much lower in the Hotan and Yarkant catchments (up to −75%). This is in-line with the extremely low precipitation found in these catchments for the GPCC (cf. Table 4) that clearly constrain the evapotranspiration in this model run. The SWIM-G internal parameter uncertainty is relatively small (below ±5%). Considering the precipitation correction of 1.5–4.3 times the observational dataset, these uncertainty ranges are acceptable.

To reduce uncertainties further and corroborate existing estimates, the existing meteorological stations network at higher elevations in the Tarim headwaters as well as all of High Asia needs to be extended (Bolch et al. 2012; Mountain Research Initiative EDW Working Group 2015; Immerzeel et al. 2014). Better incorporation of satellite observations of precipitation is also promising, but suitable datasets have only been developed recently and do not extend as far into the past. For example, the high-resolution precipitation dataset from the GPM network, which we demonstrated the potential of in our comparison with other datasets, has only been operational since 2014 (Hou et al. 2014), but promises to be useful especially for the spatial distribution of precipitation (and probably less for absolute magnitudes). Synthesizing different types of observations has already shown to be useful, for example, using gauge, radar, and satellite data (Nelson et al. 2010). Similarly, information about glaciers combined with hydrological records should be considered in mountainous regions.

b. *Precipitation correction by means of glacio-hydrological models*

Our results compare well with similar studies. For example, Immerzeel et al. (2015) find similar discrepancies with existing datasets, such as APHRODITE or TRMM-based products in the neighboring upper Indus basin, southwest of the Yarkant and Hotan catchments. Similar to our results, they obtain corrected precipitation of around 800–1200 mm a^{-1} along the Karakoram range, with similar correction factors of up to 10 for the APHRODITE dataset. They also find much drier conditions at the southeastern edge of the Yarkant catchment and south of the Wuluwati (Hotan) catchment with similar precipitation totals of 200–500 mm a^{-1}. Parameter uncertainties also compare well around the Karakoram between 10% and 50% (35% mean).

Similarly high correction factors were found by Sakai et al. (2015), who use a glacier mass balance model of

High Asian glaciers and correct the APHRODITE by tuning the model to independently estimated equilibrium line altitudes. But the relatively coarse model resolution (0.5°) fails to represent the heterogeneity of the terrain and is based on the assumption that glacier median elevation represents the equilibrium line altitude.

Although our and the two above approaches differ in time covered, model, and calibration strategy, the results provide new insights into poorly gauged and investigated catchments and reduce the uncertainty for future modeling studies. They highlight the importance of in situ and geodetic glaciological measurements of both glacier outlines and mass balance. While not immediately obvious, they are vital to constrain models that provide a greater understanding and management tools for downstream communities. Our approach has particular merit in other catchments with only discharge observations and preferably geodetic mass balance estimates available.

Some uncertainties remain in the calibration strategy and model structure, but we attempt to quantify them through a calibration ensemble (Fig. 12). We addressed parameter conflicts due to better correlation of discharge with snow/ice melt than precipitation by using agreement in annual discharge as one objective function. Incorporating snow cover maps in the automatic calibration, as was done by Duethmann et al. (2014), could further reduce the parameter uncertainty, but was outside the scope of this study. Temporal changes in correction factors as well as valley and slope specific precipitation patterns were also not considered. This would likely require a greater coupling of a high-resolution climate model (such as the HAR dataset) with the glaciological model.

c. *Mass balances in the Hotan and Yarkant catchments*

Despite the uncertainty about mass balances in the Hotan and Yarkant catchments, the parameter uncertainty of our precipitation correction with three reasonable mass balance assumptions is lower than the overall parameter uncertainty. Differences over the simulation period between the three scenarios are most significant in simulated mass balance, precipitation, and snowfall. Under all scenarios glacier mass balances are positive over the simulation period, although not in every year.

Despite a general trend of glacier recession in High Asia, glaciers in the Karakoram (Yarkant) and Kunlun Shan (Hotan) have shown strong signs of opposing this trend (sometimes referred to as the Karakoram anomaly). Hewitt (2005) show many advancing and thickening glacier tongues in the Karakoram in the late 1990s, and Liu et al. (2006) find evidence of advancing glaciers in the Kunlun Shan between 1968 and 1999. Recent investigations in the Karakoram based on declassified satellite imagery (Hexagon KH-9) from the 1970s indicate stable conditions or only slight mass loss: Bolch et al. (2017) find mass balance of -0.01 ± 0.09 m w.e. a^{-1} over 1973–99 and -0.08 ± 0.21 m w.e. a^{-1} over 1999~2009 for the Hunza catchment. For the central Karakoram, Zhou et al. (2017) give a mass balance of -0.04 ± 0.05 m w.e. a^{-1} (1973–2000). Similar findings were made for the Mutztagh Ata massif (eastern Pamir) in the north of the Yarkant catchment (Holzer et al. 2015). Studies of changes in the 2000s using ICESat satellite measurements show a positive trend in the Kunlun Shan and Tarim part of the Karakoram with mass balances of 0.03 ± 0.25 m w.e. a^{-1} (2003–09; Neckel et al. 2014), 0.05 ± 0.07 m w.e. a^{-1} (2003–08; Kääb et al. 2015), and 0.17 ± 0.15 m w.e. a^{-1} (2000–10; Gardelle et al. 2013). Brun et al. (2017) report a change of $+0.14 \pm 0.08$ m w.e. a^{-1} for Kunlun Shan (2000–16). The strengthening of the westerlies is assumed to be the cause of these stable conditions (Yao et al. 2012). In combination with the extremely high elevations, increases in precipitation lead to greater glacier accumulation even with slightly increasing temperatures (Hewitt 2005).

In light of these studies, the stable or increasing mass trends simulated here (Fig. 8) are reasonable. Although spatial and temporal domains vary, the lower initial mass balance assumption of -0.1 m w.e. a^{-1} is the most likely scenario with 0.03 ± 0.04 m w.e. a^{-1} and 0.05 ± 0.06 m w.e. a^{-1} for the Hotan and Yarkant catchments, respectively, over the period 1975–2000.

5. Conclusions

We compare six available precipitation datasets for the five major, highly glacierized headwaters of the Tarim River, northwest China. The analysis of six datasets exposes large disparities between different types, with direct observation-based datasets much lower than satellite-based or climate model-based estimates. Runoff coefficients above one support the assumption that the APHRODITE precipitation is strongly underestimating catchment-wide precipitation, especially in the data-scarce catchments of the Hotan and Yarkant rivers.

We provide a precipitation correction for the five catchments by optimizing an integrated glacier dynamics and hydrological model to observed daily and annual discharge as well as glacier area and mass balances. Satisfactory model performance suggests actual precipitation must be higher by factors of 1.5–4.3 on average to support the observed glacier area and attaining

reasonable mass balances for the reference period 1971–2000. Although high uncertainty ranges are still present (especially in areas with sparse glacier cover), the calibration ensemble represents a hydrologically and glaciologically consistent correction. The results are indicative of data discrepancies across High Asia and other sparsely gauged mountainous regions.

Acknowledgments. This study was conducted within the project SuMaRiO (Sustainable Management of River Oases along the Tarim River; http://www.sumario.de/), funded by the German Federal Ministry of Education and Research (BMBF Grants 01LL0918J and 01LL0918B). T. Bolch acknowledges funding by Deutsche Forschungsgemeinschaft (DFG, Code BO3199/2-1).

REFERENCES

Adam, J. C., E. A. Clark, D. P. Lettenmaier, and E. F. Wood, 2006: Correction of global precipitation products for orographic effects. *J. Climate*, **19**, 15–38, https://doi.org/10.1175/JCLI3604.1.

Aizen, V., E. Aizen, and J. Melack, 1995: Climate, snow cover, glaciers, and runoff in the Tien Shan, central Asia. *J. Amer. Water Resour. Assoc.*, **31**, 1113–1129, https://doi.org/10.1111/j.1752-1688.1995.tb03426.x.

Barry, R. G., 2008: *Mountain Weather and Climate.* 3rd ed., Cambridge University Press, 532 pp.

Beniston, M., 2006: Mountain weather and climate: A general overview and a focus on climatic change in the Alps. *Hydrobiologia*, **562**, 3–16, https://doi.org/10.1007/s10750-005-1802-0.

Beume, N., B. Naujoks, and M. Emmerich, 2007: SMS-EMOA: Multiobjective selection based on dominated hypervolume. *Eur. J. Oper. Res.*, **181**, 1653–1669, https://doi.org/10.1016/j.ejor.2006.08.008.

Böhner, J., 2006: General climatic controls and topoclimatic variations in central and high Asia. *Boreas*, **35**, 279–295, https://doi.org/10.1080/03009480500456073.

Bolch, T., 2017: Hydrology: Asian glaciers are a reliable water source. *Nature*, **545**, 161–162, https://doi.org/10.1038/545161a.

——, and Coauthors, 2012: The state and fate of Himalayan glaciers. *Science*, **336**, 310–314, https://doi.org/10.1126/science.1215828.

——, T. Pieczonka, K. Mukherjee, and J. Shea, 2017: Brief communication: Glaciers in the Hunza catchment (Karakoram) have been nearly in balance since the 1970s. *Cryosphere*, **11**, 531–539, https://doi.org/10.5194/tc-11-531-2017.

Bookhagen, B., and D. W. Burbank, 2006: Topography, relief, and TRMM-derived rainfall variations along the Himalaya. *Geophys. Res. Lett.*, **33**, L08405, https://doi.org/10.1029/2006GL026037.

Brun, F., E. Berthier, P. Wagnon, A. Kääb, and D. Treichler, 2017: A spatially resolved estimate of High Mountain Asia glacier mass balances from 2000 to 2016. *Nat. Geosci.*, **10**, 668–673, https://doi.org/10.1038/ngeo2999.

Changchun, X., C. Yaning, L. Weihong, C. Yapeng, and G. Hongtao, 2008: Potential impact of climate change on snow cover area in the Tarim River basin. *Environ. Geol.*, **53**, 1465–1474, https://doi.org/10.1007/s00254-007-0755-1.

Chen, Y., K. Takeuchi, C. Xu, Y. Chen, and Z. Xu, 2006: Regional climate change and its effects on river runoff in the Tarim Basin, China. *Hydrol. Processes*, **20**, 2207–2216, https://doi.org/10.1002/hyp.6200.

Clarke, G. K. C., A. H. Jarosch, F. S. Anslow, V. Radić, and B. Menounos, 2015: Projected deglaciation of western Canada in the twenty-first century. *Nat. Geosci.*, **8**, 372–377, https://doi.org/10.1038/ngeo2407.

Dee, D. P., and Coauthors, 2011: The ERA-Interim reanalysis: Configuration and performance of the data assimilation system. *Quart. J. Roy. Meteor. Soc.*, **137**, 553–597, https://doi.org/10.1002/qj.828.

De Jong, C., M. Mundelius, and K. Migała, 2005: Comparison of evapotranspiration and condensation measurements between the Giant Mountains and the Alps. *Climate and Hydrology in Mountain Areas*, C. de Jong, D. Collins, and R. Ranzi, Eds., John Wiley & Sons, 161–183, https://doi.org/10.1002/0470858249.ch12.

Duethmann, D., J. Zimmer, A. Gafurov, A. Güntner, D. Kriegel, B. Merz, and S. Vorogushyn, 2013: Evaluation of areal precipitation estimates based on downscaled reanalysis and station data by hydrological modelling. *Hydrol. Earth Syst. Sci.*, **17**, 2415–2434, https://doi.org/10.5194/hess-17-2415-2013.

——, J. Peters, T. Blume, S. Vorogushyn, and A. Güntner, 2014: The value of satellite-derived snow cover images for calibrating a hydrological model in snow-dominated catchments in Central Asia. *Water Resour. Res.*, **50**, 2002–2021, https://doi.org/10.1002/2013WR014382.

——, and Coauthors, 2015: Attribution of streamflow trends in snow- and glacier melt dominated catchments of the Tarim River, central Asia. *Water Resour. Res.*, **51**, 4727–4750, https://doi.org/10.1002/2014WR016716.

Dyurgerov, M. B., 2010: Reanalysis of Glacier Changes: From the IGY to the IPY, 1960–2008. *Mater. Glyatsiologicheskikh Issledovanij*, **108**, 5–116.

Emmerich, M., N. Beume, and B. Naujoks, 2005: An EMO algorithm using the hypervolume measure as selection criterion. *Evolutionary Multi-Criterion Optimization*, C. A. Coello Coello, A. Hernández Aguirre, and E. Zitzler, Eds., Lecture Notes in Computer Science, Vol 3410, Springer, 62–76, https://doi.org/10.1007/978-3-540-31880-4_5.

Fan, Y., Y. Chen, W. Li, H. Wang, and X. Li, 2011: Impacts of temperature and precipitation on runoff in the Tarim River during the past 50 years. *J. Arid Land*, **3**, 220–230, https://doi.org/10.3724/SP.J.1227.2011.00220.

Farinotti, D., L. Longuevergne, G. Moholdt, D. Duethmann, T. Mölg, T. Bolch, S. Vorogushyn, and A. Güntner, 2015: Substantial glacier mass loss in the Tien Shan over the past 50 years. *Nat. Geosci.*, **8**, 716–722, https://doi.org/10.1038/ngeo2513.

Feike, T., Y. Mamitimin, L. Li, and R. Doluschitz, 2015: Development of agricultural land and water use and its driving forces along the Aksu and Tarim River, P.R. China. *Environ. Earth Sci.*, **73**, 517–531, https://doi.org/10.1007/s12665-014-3108-x.

Ficklin, D. L., B. L. Barnhart, J. H. Knouft, I. T. Stewart, E. P. Maurer, S. L. Letsinger, and G. W. Whittaker, 2014: Climate change and stream temperature projections in the Columbia River basin: Habitat implications of spatial variation in hydrologic drivers. *Hydrol. Earth Syst. Sci.*, **18**, 4897–4912, https://doi.org/10.5194/hess-18-4897-2014.

Frei, C., and C. Schär, 1998: A precipitation climatology of the Alps from high-resolution rain-gauge observations. *Int. J. Climatol.*,

18, 873–900, https://doi.org/10.1002/(SICI)1097-0088(19980630)18:8<873::AID-JOC255>3.0.CO;2-9.

Frey, H., and Coauthors, 2014: Estimating the volume of glaciers in the Himalayan–Karakoram region using different methods. *Cryosphere*, **8**, 2313–2333, https://doi.org/10.5194/tc-8-2313-2014.

Gardelle, J., E. Berthier, Y. Arnaud, and A. Kääb, 2013: Region-wide glacier mass balances over the Pamir-Karakoram-Himalaya during 1999–2011. *Cryosphere*, **7**, 1263–1286, https://doi.org/10.5194/tc-7-1263-2013.

Gascoin, S., C. Kinnard, R. Ponce, S. Lhermitte, S. MacDonell, and A. Rabatel, 2011: Glacier contribution to streamflow in two headwaters of the Huasco River, Dry Andes of Chile. *Cryosphere*, **5**, 1099–1113, https://doi.org/10.5194/tc-5-1099-2011.

Glazirin, G., 2010: A century of investigations on outbursts of the ice-dammed Lake Merzbacher (central Tien Shan). *Austrian J. Earth Sci.*, **103**, 171–179.

Goel, M. K., 2011: Runoff coefficient. *Encyclopedia of Snow, Ice and Glaciers*, V. P. Singh, P. Singh, and U. K. Haritashya, Eds., Encyclopedia of Earth Sciences Series, Springer, 952–953.

Groisman, P. Y., V. V. Koknaeva, T. A. Belokrylova, and T. R. Karl, 1991: Overcoming biases of precipitation measurement: A history of the USSR experience. *Bull. Amer. Meteor. Soc.*, **72**, 1725–1733, https://doi.org/10.1175/1520-0477(1991)072<1725:OBOPMA>2.0.CO;2.

Haddeland, I., and Coauthors, 2011: Multimodel estimate of the global terrestrial water balance: Setup and first results. *J. Hydrometeor.*, **12**, 869–884, https://doi.org/10.1175/2011JHM1324.1.

Henn, B., M. P. Clark, D. Kavetski, and J. D. Lundquist, 2015: Estimating mountain basin-mean precipitation from streamflow using Bayesian inference. *Water Resour. Res.*, **51**, 8012–8033, https://doi.org/10.1002/2014WR016736.

——, ——, ——, B. McGurk, T. H. Painter, and J. D. Lundquist, 2016: Combining snow, streamflow, and precipitation gauge observations to infer basin-mean precipitation. *Water Resour. Res.*, **52**, 8700–8723, https://doi.org/10.1002/2015WR018564.

——, A. J. Newman, B. Livneh, C. Daly, and J. D. Lundquist, 2018: An assessment of differences in gridded precipitation datasets in complex terrain. *J. Hydrol.*, **556**, 1205–1219, https://doi.org/10.1016/j.jhydrol.2017.03.008.

Hewitt, K., 2005: The Karakoram anomaly? Glacier expansion and the 'elevation effect,' Karakoram Himalaya. *Mt. Res. Dev.*, **25**, 332–340, https://doi.org/10.1659/0276-4741(2005)025[0332:TKAGEA]2.0.CO;2.

Hock, R., and B. Holmgren, 2005: A distributed surface energy-balance model for complex topography and its application to Storglaciären, Sweden. *J. Glaciol.*, **51**, 25–36, https://doi.org/10.3189/172756505781829566.

Holzer, N., S. Vijay, T. Yao, B. Xu, M. Buchroithner, and T. Bolch, 2015: Four decades of glacier variations at Muztagh Ata (eastern Pamir): A multi-sensor study including Hexagon KH-9 and Pléiades data. *Cryosphere*, **9**, 2071–2088, https://doi.org/10.5194/tc-9-2071-2015.

Hou, A. Y., and Coauthors, 2014: The Global Precipitation Measurement Mission. *Bull. Amer. Meteor. Soc.*, **95**, 701–722, https://doi.org/10.1175/BAMS-D-13-00164.1.

Huffman, G. J., 2006: Satellite-based estimation of precipitation using microwave sensors. *Encyclopedia of Hydrological Sciences*, M. G. Anderson and J. J. McDonnell, Eds., John Wiley & Sons, https://doi.org/10.1002/0470848944.hsa055.

——, E. F. Stocker, D. Bolvin, and E. Nelkin, 2014: 3IMERGM data set. NASA GSFC, accessed 12 October 2016, https://pmm.nasa.gov/GPM.

Huss, M., R. Hock, A. Bauder, and M. Funk, 2010: 100-year mass changes in the Swiss Alps linked to the Atlantic Multidecadal Oscillation. *Geophys. Res. Lett.*, **37**, L10501, https://doi.org/10.1029/2010GL042616.

Immerzeel, W. W., L. P. H. van Beek, M. Konz, A. B. Shrestha, and M. F. P. Bierkens, 2012a: Hydrological response to climate change in a glacierized catchment in the Himalayas. *Climatic Change*, **110**, 721–736, https://doi.org/10.1007/s10584-011-0143-4.

——, F. Pellicciotti, and A. B. Shrestha, 2012b: Glaciers as a proxy to quantify the spatial distribution of precipitation in the Hunza Basin. *Mt. Res. Dev.*, **32**, 30–38, https://doi.org/10.1659/MRD-JOURNAL-D-11-00097.1.

——, L. Petersen, S. Ragettli, and F. Pellicciotti, 2014: The importance of observed gradients of air temperature and precipitation for modeling runoff from a glacierized watershed in the Nepalese Himalayas. *Water Resour. Res.*, **50**, 2212–2226, https://doi.org/10.1002/2013WR014506.

——, N. Wanders, A. F. Lutz, J. M. Shea, and M. F. P. Bierkens, 2015: Reconciling high-altitude precipitation in the upper Indus basin with glacier mass balances and runoff. *Hydrol. Earth Syst. Sci.*, **19**, 4673–4687, https://doi.org/10.5194/hess-19-4673-2015.

Kääb, A., D. Treichler, C. Nuth, and E. Berthier, 2015: Brief Communication: Contending estimates of 2003–2008 glacier mass balance over the Pamir–Karakoram–Himalaya. *Cryosphere*, **9**, 557–564, https://doi.org/10.5194/tc-9-557-2015.

Kaser, G., M. Großhauser, and B. Marzeion, 2010: Contribution potential of glaciers to water availability in different climate regimes. *Proc. Natl. Acad. Sci. USA*, **107**, 20 223–20 227, https://doi.org/10.1073/pnas.1008162107.

Kochendorfer, J., and Coauthors, 2017: The quantification and correction of wind-induced precipitation measurement errors. *Hydrol. Earth Syst. Sci.*, **21**, 1973–1989, https://doi.org/10.5194/hess-21-1973-2017.

Krysanova, V., and Coauthors, 2015: Analysis of current trends in climate parameters, river discharge and glaciers in the Aksu River basin (central Asia). *Hydrol. Sci. J.*, **60**, 566–590, https://doi.org/10.1080/02626667.2014.925559.

Liu, X., Q. Yang, and Y. Liang, 2006: Study on the change of runoff and the effect factors in the Aksu River basin in recent 40 years. *China Popul. Resour. Environ.*, **16** (3), 83–87.

Liu, Z., 2015: Comparison of precipitation estimates between Version 7 3-hourly TRMM Multi-Satellite Precipitation Analysis (TMPA) near-real-time and research products. *Atmos. Res.*, **153**, 119–133, https://doi.org/10.1016/j.atmosres.2014.07.032.

Lorenz, C., and H. Kunstmann, 2012: The hydrological cycle in three state-of-the-art reanalyses: Intercomparison and performance analysis. *J. Hydrometeor.*, **13**, 1397–1420, https://doi.org/10.1175/JHM-D-11-088.1.

Lutz, A. F., W. W. Immerzeel, A. B. Shrestha, and M. F. P. Bierkens, 2014: Consistent increase in High Asia's runoff due to increasing glacier melt and precipitation. *Nat. Climate Change*, **4**, 587–592, https://doi.org/10.1038/nclimate2237.

Marshall, S. J., E. C. White, M. N. Demuth, T. Bolch, R. Wheate, B. Menounos, M. J. Beedle, and J. M. Shea, 2011: Glacier water resources on the eastern slopes of the Canadian Rocky Mountains. *Can. Water Resour. J.*, **36**, 109–134, https://doi.org/10.4296/cwrj3602823.

Maussion, F., D. Scherer, T. Mölg, E. Collier, J. Curio, and R. Finkelnburg, 2014: Precipitation seasonality and variability over the Tibetan Plateau as resolved by the High Asia Reanalysis. *J. Climate*, **27**, 1910–1927, https://doi.org/10.1175/JCLI-D-13-00282.1.

Mölg, T., N. J. Cullen, and G. Kaser, 2009: Solar radiation, cloudiness and longwave radiation over low-latitude glaciers: Implications for mass-balance modelling. *J. Glaciol.*, **55**, 292–302, https://doi.org/10.3189/002214309788608822.

——, F. Maussion, and D. Scherer, 2014: Mid-latitude westerlies as a driver of glacier variability in monsoonal High Asia. *Nat. Climate Change*, **4**, 68–73, https://doi.org/10.1038/nclimate2055.

Mountain Research Initiative EDW Working Group, 2015: Elevation-dependent warming in mountain regions of the world. *Nat. Climate Change*, **5**, 424–430, https://doi.org/10.1038/nclimate2563.

Mu, Q., F. A. Heinsch, M. Zhao, and S. W. Running, 2007: Development of a global evapotranspiration algorithm based on MODIS and global meteorology data. *Remote Sens. Environ.*, **111**, 519–536, https://doi.org/10.1016/j.rse.2007.04.015.

Nash, J., and J. Sutcliffe, 1970: River flow forecasting through conceptual models part I—A discussion of principles. *J. Hydrol.*, **10**, 282–290, https://doi.org/10.1016/0022-1694(70)90255-6.

Neckel, N., J. Kropáček, T. Bolch, and V. Hochschild, 2014: Glacier mass changes on the Tibetan Plateau 2003–2009 derived from ICESat laser altimetry measurements. *Environ. Res. Lett.*, **9**, 014009, https://doi.org/10.1088/1748-9326/9/1/014009.

Nelson, B. R., D.-J. Seo, and D. Kim, 2010: Multisensor Precipitation Reanalysis. *J. Hydrometeor.*, **11**, 666–682, https://doi.org/10.1175/2010JHM1210.1.

Osmonov, A., T. Bolch, C. Xi, A. Kurban, and W. Guo, 2013: Glacier characteristics and changes in the Sary-Jaz River basin (central Tien Shan, Kyrgyzstan)—1990–2010. *Remote Sens. Lett.*, **4**, 725–734, https://doi.org/10.1080/2150704X.2013.789146.

Peters, J., T. Bolch, A. Gafurov, and N. Prechtel, 2015: Snow cover distribution in the Aksu Catchment (central Tien Shan) 1986–2013 based on AVHRR and MODIS data. *IEEE J. Sel. Top. Appl. Earth Obs. Remote Sens.*, **8**, 5361–5375, https://doi.org/10.1109/JSTARS.2015.2477108.

Pieczonka, T., and T. Bolch, 2015: Region-wide glacier mass budgets and area changes for the central Tien Shan between ~1975 and 1999 using Hexagon KH-9 imagery. *Global Planet. Change*, **128**, 1–13, https://doi.org/10.1016/j.gloplacha.2014.11.014.

Pritchard, H. D., 2017: Asia's glaciers are a regionally important buffer against drought. *Nature*, **545**, 169–174, https://doi.org/10.1038/nature22062.

Ragettli, S., F. Pellicciotti, R. Bordoy, and W. W. Immerzeel, 2013: Sources of uncertainty in modeling the glaciohydrological response of a Karakoram watershed to climate change. *Water Resour. Res.*, **49**, 6048–6066, https://doi.org/10.1002/wrcr.20450.

Rockel, B., A. Will, and A. Hense, 2008: Regional climate modelling with COSMO-CLM (CCLM). *Meteor. Z.*, **17**, 347–348, https://doi.org/10.1127/0941-2948/2008/0309.

Rumbaur, C., and Coauthors, 2015: Sustainable management of river oases along the Tarim River (SuMaRiO) in northwest China under conditions of climate change. *Earth Syst. Dynam.*, **6**, 83–107, https://doi.org/10.5194/esd-6-83-2015.

Sakai, A., T. Nuimura, K. Fujita, S. Takenaka, H. Nagai, and D. Lamsal, 2015: Climate regime of Asian glaciers revealed by GAMDAM glacier inventory. *Cryosphere*, **9**, 865–880, https://doi.org/10.5194/tc-9-865-2015.

Schneider, U., A. Becker, P. Finger, A. Meyer-Christoffer, B. Rudolf, and M. Ziese, 2015: GPCC Full Data Reanalysis Version 7.0 at 0.5: Monthly land-surface precipitation from rain-gauges built on GTS-based and historic data. Global Precipitation Climatology Centre at Deutscher Wetterdienst, accessed 18 July 2016, ftp://ftp.dwd.de/pub/data/gpcc/html/fulldata_v7_doi_download.html.

Sevruk, B., 1985: Systematischer Niederschlagsmessfehler in der Schweiz. *Beitr. Geol. Schweiz Hydrol.*, **31**, 65–75.

——, and K. Mieglitz, 2002: The effect of topography, season and weather situation on daily precipitation gradients in 60 Swiss valleys. *Water Sci. Technol.*, **45**, 41–48.

Shangguan, D., and Coauthors, 2007: Glacier changes in the west Kunlun Shan from 1970 to 2001 derived from Landsat TM/ETM+ and Chinese glacier inventory data. *Ann. Glaciol.*, **46**, 204–208, https://doi.org/10.3189/172756407782871693.

Smith, E. A., and Coauthors, 2007: International Global Precipitation Measurement (GPM) program and mission: An overview. *Measuring Precipitation From Space*, V. Levizzani, P. Bauer, and F. J. Turk, Eds., Advances In Global Change Research, No. 28, Springer, 611–653.

Sorg, A., T. Bolch, M. Stoffel, O. Solomina, and M. Beniston, 2012: Climate change impacts on glaciers and runoff in Tien Shan (Central Asia). *Nat. Climate Change*, **2**, 725–731, https://doi.org/10.1038/nclimate1592.

Stagge, J. H., and G. E. Moglen, 2014: Evolutionary algorithm optimization of a multireservoir system with long lag times. *J. Hydrol. Eng.*, **19**, https://doi.org/10.1061/(ASCE)HE.1943-5584.0000972.

Stisen, S., A. L. Højberg, L. Troldborg, J. C. Refsgaard, B. S. B. Christensen, M. Olsen, and H. J. Henriksen, 2012: On the importance of appropriate precipitation gauge catch correction for hydrological modelling at mid to high latitudes. *Hydrol. Earth Syst. Sci.*, **16**, 4157–4176, https://doi.org/10.5194/hess-16-4157-2012.

Tao, H., M. Gemmer, Y. Bai, B. Su, and W. Mao, 2011: Trends of streamflow in the Tarim River basin during the past 50 years: Human impact or climate change? *J. Hydrol.*, **400**, 1–9, https://doi.org/10.1016/j.jhydrol.2011.01.016.

Thevs, N., 2011: Water scarcity and allocation in the Tarim basin: Decision structures and adaptations on the local level. *J. Curr. Chin. Aff.*, **40**, 113–137, https://d-nb.info/102441566X/34.

Tong, K., F. Su, D. Yang, L. Zhang, and Z. Hao, 2014: Tibetan Plateau precipitation as depicted by gauge observations, reanalyses and satellite retrievals. *Int. J. Climatol.*, **34**, 265–285, https://doi.org/10.1002/joc.3682.

Valéry, A., V. Andréassian, and C. Perrin, 2009: Inverting the hydrological cycle: When streamflow measurements help assess altitudinal precipitation gradients in mountain areas. *IAHS Publ.*, **333**, 281–286.

Wang, G., Y. Shen, H. Su, J. Wang, W. Mao, Q. Gao, and S. Wang, 2008: Runoff changes in Aksu River basin during 1956–2006 and their impacts on water availability for Tarim River. *J. Glaciol. Geocryology*, **30** (4), 562–568.

Wang, Y., Ed., 2006: *Local Records of the Aksu River Basin* (in Chinese). Fangshi Publisher, 88 pp.

Weedon, G. P., and Coauthors, 2011: Creation of the WATCH forcing data and its use to assess global and regional reference crop evaporation over land during the twentieth century. *J. Hydrometeor.*, **12**, 823–848, https://doi.org/10.1175/2011JHM1369.1.

Winiger, M., M. Gumpert, and H. Yamout, 2005: Karakorum–Hindukush–western Himalaya: Assessing high-altitude water resources. *Hydrol. Processes*, **19**, 2329–2338, https://doi.org/10.1002/hyp.5887.

Winkler, M., I. Juen, T. Mölg, P. Wagnon, J. Gómez, and G. Kaser, 2009: Measured and modelled sublimation on the

tropical Glaciar Artesonraju, Perú. *Cryosphere*, **3**, 21–30, https://doi.org/10.5194/tc-3-21-2009.

Wortmann, M., V. Krysanova, Z. W. Kundzewicz, B. Su, and X. Li, 2014: Assessing the influence of the Merzbacher Lake outburst floods on discharge using the hydrological model SWIM in the Aksu headwaters, Kyrgyzstan/NW China. *Hydrol. Processes*, **28**, 6337–6350, https://doi.org/10.1002/hyp.10118.

——, T. Bolch, V. Krysanova, and S. Buda, 2016: Bridging glacier and river catchment scales: An efficient representation of glacier dynamics in a hydrological model. *Hydrol. Earth Syst. Sci. Discuss.*, https://doi.org/10.5194/hess-2016-272.

Yang, D., and T. Ohata, 2001: A bias-corrected Siberian regional precipitation climatology. *J. Hydrometeor.*, **2**, 122–139, https://doi.org/10.1175/1525-7541(2001)002<0122:ABCSRP>2.0.CO;2.

——, and Coauthors, 1999: Wind-induced precipitation undercatch of the Hellmann gauges. *Hydrol. Res.*, **30**, 57–80, http://hr.iwaponline.com/content/30/1/57.

Yao, T., and Coauthors, 2012: Different glacier status with atmospheric circulations in Tibetan Plateau and surroundings. *Nat. Climate Change*, **2**, 663–667, https://doi.org/10.1038/nclimate1580.

Yatagai, A., K. Kamiguchi, O. Arakawa, A. Hamada, N. Yasutomi, and A. Kitoh, 2012: APHRODITE: Constructing a long-term daily gridded precipitation dataset for Asia based on a dense network of rain gauges. *Bull. Amer. Meteor. Soc.*, **93**, 1401–1415, https://doi.org/10.1175/BAMS-D-11-00122.1.

You, Q., K. Fraedrich, G. Ren, B. Ye, X. Meng, and S. Kang, 2012: Inconsistencies of precipitation in the eastern and central Tibetan Plateau between surface adjusted data and reanalysis. *Theor. Appl. Climatol.*, **109**, 485–496, https://doi.org/10.1007/s00704-012-0594-1.

Zemp, M., M. Hoelzle, and W. Haeberli, 2009: Six decades of glacier mass-balance observations: A review of the worldwide monitoring network. *Ann. Glaciol.*, **50**, 101–111, https://doi.org/10.3189/172756409787769591.

Zhou, Y., Z. Li, and J. Li, 2017: Slight glacier mass loss in the Karakoram region during the 1970s to 2000 revealed by KH-9 images and SRTM DEM. *J. Glaciol.*, **63**, 331–342, https://doi.org/10.1017/jog.2016.142.